Check for updates

Copper inks for printed electronics: a review

Xianghui Zeng, Pei He, [ID] * Minglu Hu, Weikai Zhao, Huitong Chen, Longhui Liu, Jia Sun [ID] and Junliang Yang [ID] *

Conductive inks have attracted tremendous attention owing to their adaptability and the convenient large-scale fabrication. As a new type of conductive ink, copper-based ink is considered to be one of the best candidate materials for the conductive layer in flexible printed electronics owing to its high conductivity and low price, and suitability for large-scale manufacturing processes. Recently, tremendous progress has been made in the preparation of cooper-based inks for electronic applications, but the antioxidation ability of copper-based nanomaterials within inks or films, that is, long-term reliability upon exposure to water and oxygen, still needs more exploration. In this review, we present a comprehensive overview of copper inks for printed electronics from ink preparation, printing methods and sintering, to antioxidation strategies and electronic applications. The review begins with an overview of the development of copper inks, followed by a demonstration of various preparation methods for copper inks. Then, the diverse printing techniques and post-annealing strategies used to fabricate conductive copper patterns are discussed. In addition, antioxidation strategies utilized to stabilize the mechanical and electrical properties of copper nanomaterials are summarized. Then the diverse applications of copper inks for electronic devices, such as transparent conductive electrodes, sensors, optoelectronic devices, and thin-film transistors, are discussed. Finally, the future development of copper-based inks and the challenges of their application in printed electronics are discussed.

1. Introduction

The next-generation electronic devices (e-devices) are developing in the direction of wearables, and their advantages of light weight and portability are attracting increasing attention.[1–3] The failure strain of monocrystalline silicon being less than 2%,[4] so many silicon-based devices have poor ductility with high weight, which makes it difficult to adapt them to the requirements of flexibility and portability for wearable e-devices.[5–7] At the same time, the high demand combined with the complexity of the traditional device preparation process make it difficult to achieve mass production at a low price.[8–10] Printed electronics (PE) technology, which combines traditional printing technology with electronic manufacturing, often uses solution methods to prepare customized patterns through printing.[11–13] Owing to the advantages of little waste of materials and a simple process, PE technology has been widely used in the large-scale preparation of electronic devices.[14] Meanwhile, the printing process can be used to prepare electronic circuits and devices on different substrates, breaking the limitations of tra-

ditional silicon-based circuits, and the prepared devices have the characteristics of light weight, low cost, and bending resistance, promoting the development of the next generation of intelligent electronic devices.[15–19]

Conductive inks are one of the most important functional materials in printed electronic devices, and their properties determine the methods of printing and annealing. In recent years, many conductive ink materials have been developed, such as graphene,[20–23] carbon nanotubes,[24–26] metal nanoparticles,[27–29] and conductive polymers.[30–32] Although organic polymers have good ductility and robustness, their conductivity is poor, necessitating additional fillers and doping to meet the application requirements. Graphene has no band gap, but only the ideal two-dimensional monolayer structure has good conductivity. In contrast, metallic materials with high intrinsic conductivity (Au ~2.44 μΩ cm, Ag ~1.59 μΩ cm, Cu ~1.68 μΩ cm, Al ~2.65 μΩ cm, Ni ~6.99 μΩ cm) have great potential in low-power transmission and sensing.[33] As an inert metal, gold generally does not react with other substances, and is widely used in TFTs and solar cells.[34–37] However, its high price restricts its use for ink printing. As an alternative to gold, silver shows high conductivity and good fineness, and can be applied to a variety of printing methods,[38,39] but its low electromigration resistance makes it prone to electromigration,[40] resulting in long-term stability

Hunan Key Laboratory for Super-Microstructure and Ultrafast Process, School of Physics and Electronics, Central South University, Changsha, 410083 Hunan, People's Republic of China. E-mail: pei.he@csu.edu.cn, junliang.yang@csu.edu.cn

decline, and its price is relatively expensive. Copper is abundant (more than 1000 times the content of silver), cheap (1% of the price of silver), and shows good electrical conductivity (between those of silver and gold) and thermal conductivity.[41–47]

Copper-based inks are attracting increasing attention. A large number of studies have shown that copper-based inks can achieve high conductivity through printing, which is necessary to realize the industrialized preparation of large-scale flexible electronic devices.[48–51] However, there are two obvious problems in copper-based inks, that is, the conductivity in the initial stage and long-term stability after preparation.[52,53] There are many factors affecting the conductivity, such as the specific gravity of the metal filler, the bridging between single metal particles (nanowires), and the porosity of the sintered film.[54–56] The stability is poor because copper is easily oxidized into copper oxide (CuO) and cuprous oxide (Cu_2O) when placed in air.[57–60] Therefore, how to prepare copper-based ink with low resistivity and strong oxidation resistance is a problem that people have been focusing on.

In recent years, copper-based ink has developed rapidly in the field of printing electronics, including the preparation of the ink, the improvement of the printing process, and new applications.[61–66] To improve the electrical conductivity and stability of copper film after printing, many efforts have been made to modify the ink filler, adjust the printing mode, and optimize the sintering process.[67–72] This review summarizes the recent work on copper-based inks, including the preparation and characteristics of common copper-based inks, and then the preparation of electronic devices through appropriate printing methods and sintering processes. In addition, we also introduce several methods to protect the printing plate from oxidation. Finally, we summarize the applications of copper-based ink, as shown in Fig. 1.

2. Preparation and properties of copper inks

Metal inks need to be sintered after printing to achieve neck connection between particles for conductivity. Compared with silver, the higher melting point of copper necessitates more energy during the sintering process.[28,73] However, with the increase in temperature, the oxidation of copper seriously affects its conductivity, hindering its application as a high conductivity material. More importantly, flexible substrates (such as PET, PEN, and paper) cannot exist stably at high sintering temperatures (>150 °C). Thus, to realize sintering at lower temperatures (<120 °C) and solve the oxidation problem, copper-based inks with different formulations have been developed in previous research works.[74–79] The different types of ink materials can be classified as follows: copper particle ink, copper nanowire ink, copper precursor ink, and copper mixed ink. This section discusses different formulations of copper inks and their performance.

2.1. Copper particle ink

As one of the earliest developed materials, the preparation methods for metal particles are mature, such as chemical reduction, electrochemical synthesis, and thermal treatment.[78,80–84] Micron or nanoscale particles show the unique properties of quantum size, but with the reduction of size, copper particles have a higher specific surface area, which means that they can be dispersed in solvents with a stabilizer to form conductive inks.[85] However, for copper particles, small size will make more copper element exposed to water or oxygen to form oxides (CuO, Cu_2O), which means that copper particle inks usually need to be stored in reducing solutions, such as oleic acid.[86,87] More importantly, the higher
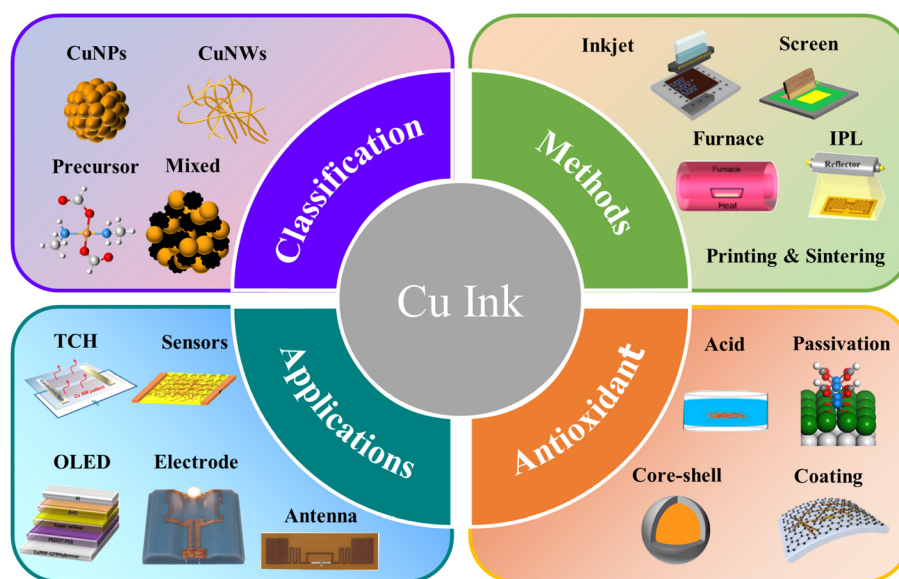

Fig. 1 Schematic diagram of the classification, fabrication, antioxidation methods and application of copper inks.

melting point of copper oxide (CuO ~1446 °C) will increase the temperature requirement for sintering. Although the synthesis of copper particles with a smaller radius can effectively reduce the temperature required for sintering,[88,89] it will also make the particles agglomerate and precipitate in the solvent,[56] resulting in nozzle blockage during the printing process. At present, the mainstream solution to increase the interaction between molecules and cover the copper particles to form a protective layer is to add capping agents of organic substances, such as polyvinylpyrrolidone (PVP),[54,56,90–92] oleic acid,[93] thiol,[94,95] oleamine,[96] cellulose[97,98] and acid.[76,99] The capping agents can be effectively desorbed during the subsequent sintering process, as shown in Fig. 2a. In addition, for different applications, additional additives (such as adhesives and surface tension modifiers) are needed to increase the adhesion between the ink and the substrate or change the shear adaptability of the ink.[79] Information for several copper particle inks in terms of the materials, capping agents, sintering methods, and resistivity is listed in Table 1.

The chemical reduction generally uses substances such as ascorbic acid[102] or hydrazine[103,104] to reduce copper-containing compounds ($Cu(NO_3)_2$,[105–107] $Cu(HCOO)_2$,[74] $CuCl_2$,[108–110] etc.) to obtain elemental copper particles (CuPs). The capping agent can achieve chemisorption in solution through the interaction of lone electron pairs between N, O and Cu, forming a barrier between Cu and the outside environment (Fig. 2b).[100] Jeong et al. synthesized copper nanoparticles (CuNPs) by polyol method, in which PVP with different molecular weights was added to the solution to control the thickness of the oxide layer on the surface of copper particles.[90] Using PVP with a molecular weight of 40 000 g mol^{-1}, the synthesized copper particles had a diameter of 60 ± 8 nm and the minimum thick-

ness of the CuO layer was 1.6 nm. PVP not only disperses the synthesized Cu particles evenly, but also improves the adhesion between the printed film and the substrate. Yokoyama et al. optimized the PVP concentration and dispersion time in the CuNPs ink and obtained the best dispersion effect and sufficiently high interface fracture energy at a concentration of 5 wt%.[91] The sintering temperature was reduced to 225 °C and the resistivity of the film was 44.7 μΩ cm. Moreover, this ink can be applied to various substrates (glass, polyimide, polyaniline, liquid crystal polymer). However, the insulation of PVP affects the conductivity of the sintering pattern, and its high molecular weight means that its removal requires a high temperature,[43] which is not applicable to substrates with a low glass transition temperature (T_g). Thus, it is necessary to find capping agents that can be decomposed at low temperature.[111]

Short-chain carboxylic acids are regarded as good capping agents because of their good oxidation resistance and low decomposition temperature.[136,137] The length of the carbon chain and the functional groups can affect the size and uniformity of the growth of copper particles. Longer carbon chains and more functional groups can improve the van der Waals interaction between molecules and produce greater cohesion, to obtain Cu with smaller particle size and better dispersion abllity.[138] Deng et al. prepared stable copper nanoparticles with particle sizes less than 10 nm with lactic acid as a capping agent.[99] The low decomposition temperature of lactic acid enables the cooper ink to turn into Cu film with a resistivity of 21.0 ± 7.0 μΩ cm after annealing at 150 °C. They also found that increasing lactic acid concentration not only reduced the size of the synthesized copper particles, but also distributed the copper particles. However, with the addition of
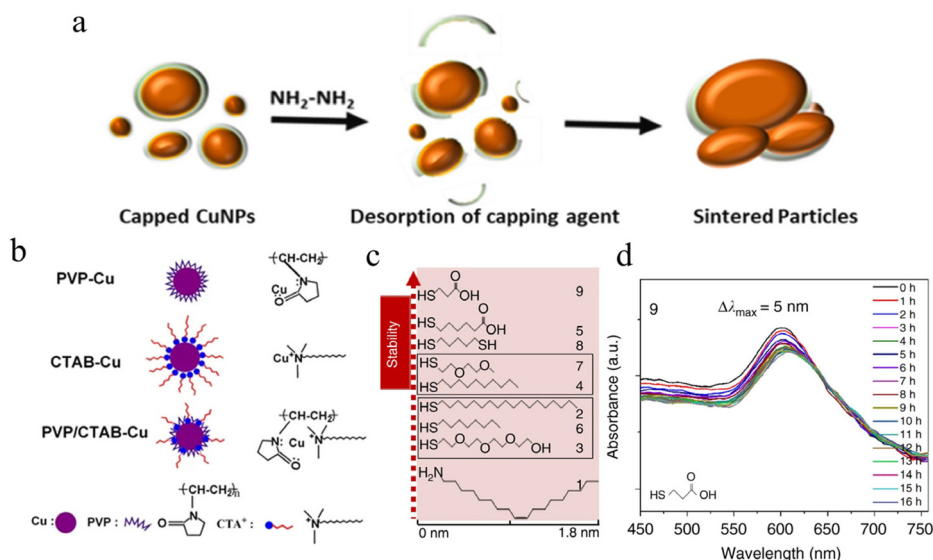

Fig. 2 (a) Schematic diagram of high-molecular-weight PVP chemisorbed on the surface of CuNPs.[76] Reproduced with permission from ref. 76. Copyright 2021 Elsevier. (b) The mechanism of PVP, CTAB, and the mix of PVP and CTAB with CuNPs.[100] Reproduced with permission from ref. 100. Copyright 2013 Springer. (c) Molecular structures of thiols according to the stability in air when used as a capping layer for CuNPs.[101] (d) The UV-vis stability of MPA-treated CuNPs.[101] Reproduced with permission from ref. 101. Copyright 2017 Springer.

Table 1 Summary of Cu particle/mixed inks detailing the materials, capping/reducing agents, substrates, sintering methods and resistivity

Material	Capping agent/reductant/additive	Substrate	Method	Post-treatment method	Resistivity (μΩ cm)	Ref.
Bulk Cu	—	—	—	—	1.68	97
CuNPLs	HPMC	Kapton	Direct writing	Formate treatment	—	112
Cu flake	Phenol resin/triethanolamine	PI	Screen	Thermal sintering (170 °C in air)	74.6	76
CuNPs	Citric acid/sodium hypophosphite	PET	Screen	Thermal sintering (60 °C in air)	744 ± 9	113
CuNPs	NA	PI	Doctor balding	Thermal sintering (250 °C H_2 in N_2)/PECVD for graphene	37.6	114
CuNPs	EC/α-terpineol	PI	Screen	IPL	9.54	75
CuNPs	NA	GaAs	Inkjet	Laser sintering	11	91
CuNPs	PVP	Glass/PI	Spin-coating	Thermal sintering (225 °C in Ar)	44.7	94
CuNPs	1-Octanethiol	Paper	Inkjet	IPL	28	74
CuNCs	BYK	Glass	Bar coating	Thermal sintering (400 °C in N_2)	23	115
CuNPs	NA	Liquid crystal polymer	Aerosol jet	IPL	—	
CuNPs	Copper acetate/2-dimethylaminoethanol	Si/SiO_2	Inkjet	Thermal sintering (250 °C in vacuum)	—	116
CuNPs	PGMEA	Si/SiO_2	EHD	Thermal sintering (380 °C in vacuum)	8×10^4	117
CuNPs	1-Octanethiol	PI	Inkjet	IPL	24	95
CuNPs	Oleic acid	PI	Air-brush	IPL	6.7	93
CuNPs	PVP/CTAB	Paper	Direct writing	Thermal sintering (160 °C in air)	11 ± 0.8	100
CuNPs	Lactic acid	Glass	Spin-coating	Thermal sintering (150 °C in N_2)	21.0 ± 7.0	99
CuNPs	PVP	PI	Spin-coating	IPL	5.2	54
CuNPs	PVP	PI	Inkjet	Thermal sintering (275 °C in vacuum)	11.6	90
CuNPs	PVP/NaH$_2$·PO$_2$·H$_2$O	Glass	Inkjet	Thermal sintering (325 °C in vacuum)	17.2	56
CuNPs	PVP/ascorbic acid	Si	Screen	Thermal sintering (400 °C in vacuum)	27	118
CuNPs/Ag	EC/α-terpineol	PET	Screen	Drying at room temperature	14	98
CuNPs/Ag	Oleylamine	Glass	Spin-coating	Thermal sintering (350 °C in vacuum)	12.0	119
CuNPs/Sn	Ascorbic acid	Scotch tape template	Spin-coating	Thermal sintering (200 °C in H_2)	164	120
CuMPs/AgNPs	PVP/EG/glycerol	PET	Screen	IPL	—	121
CuNPs/CuNWs	PVP	PI	Spin-coating	Thermal sintering (250 °C in Ar)	31.5	122
Cu flake/NiF	AmIP/EG	PI	Doctor-blading	Thermal sintering (150 °C in N_2)	51	123
CuNPs/$Cu(NO_3)_2$/Ni	PVP/DEG	PI	Doctor-blading	IPL	14.78	124
CuNPs/CuNWs	AMP/2-ethylhexylamine	PET	Screen	Thermal sintering (140 °C in N_2)	14.9	125
CuNPs/CuMPs	EC/α-terpineol	Glass	Screen	IPL	5.94	126
Cu(ii) formate/Ni(ii) formate	AMP	PI	Screen	Thermal sintering/IPL	29	127
CuNPs/CuMPs	EC	PI	Screen	IPL	6.94	128
CuMPs/AgNPs	EC/epoxy	PI	Screen	IPL	5.12	129
Cu(ii) formate/MWCNT	AMP/n-octylamine	PET	Screen	Thermal sintering (140 °C in N_2)	25.31	130
CuNPs/NiNPs	PVP/EC	PET	Screen	IPL	—	131
Cu@Sn NPs	Oleic acid	PES	Air-brush	IPL	8.2	66
Cu@Ni NPs	2-Methoxy ethanol	Glass	Mayer coating	350 °C in H_2 and Ar	27.4	68
Cu@Ni NPs	Phenylhydrazine	PI	Spray-coating	IPL	—	96
Cu(ii) formate/CuNPs	AMP	PET	Screen	Thermal sintering (140 °C in N_2)	11.3	132
CuNPs/AgNPs	PVP	PI	Doctor-blading	IPL	4.06	133
Cu@Ag NPs	Oleylamine/1-amino-2-propanol	PET	Doctor-blading	Chemical sintering (MIPA and $NaBH_4$)	36.3	134
Cu(ii) formate/silver oxalate	EG/1,2-diaminopropane	PI	Dropping	180 °C in N_2	90.56	135

more acid, the pH of the ink will decrease, which will increase the copper reduction rate, and a large number of copper cores will rapidly accumulate, converge into large pie ces and harden.[139] The purpose of capping is to make the capping agent form strong covalent bonds around Cu particles and hinder the agglomeration between particles and contact with oxygen. Therefore, in principle, a material that forms a strong covalent bond with copper is the best choice. Compared with copper–amine and copper–carboxylic acid bonds, copper–sulfur (Cu–S) bonds have stronger binding energy, so thiol solutions are the primary choice for capping.[140] However, it is reported that thiol solution as a capping agent will etch CuNPS, making this scheme undesirable.[141] Dabera *et al.* found for the first time that using mercaptan ligands with a short alkyl chain and containing hydrophilic carboxylic acid end groups can significantly reduce the oxidation rate of copper nanoparticles in the air without etching copper nanoparticles,[101] as shown in Fig. 2d. The extinction spectrum of copper nanoparticles with 3-mercaptopropionic acid (MPA) only redshifted by 5 nm after being placed in air for 16 hours, showing high antioxidant performance. At the same time, the low boiling point of MPA (111.5 °C at 2.0 kPa) also greatly reduces the temperature required for sintering. High copper content copper particle inks can produce films with low resistivity after printing and sintering, but the addition of a capping agent and the use of reducing substances can only delay the oxidation process, which means that the copper particle ink often needs to be used immediately after preparation in the application process. This limits the convenience of use.

2.2. Copper nanowire ink

During the process of synthesizing copper particles, if the ligand is limited to binding specifically to other surfaces of copper, the nano copper will be guided to grow into one-dimensional nanowires along the uniaxial direction.[41,44,48,50,142] Copper nanowires (CuNWs) have excellent mechanical toughness and an efficient electron transfer rate.[143] The contact between rods without melting to form a neck connection significantly reduces the temperature required for sintering. CuNWs are generally synthesized in solution, using either the hydrothermal method or the organic solvent method depending on the solvent environment.[144–146] Table 2 lists the materials, capping agents, sintering methods, aspect ratio, and resistivity of some CuNWs inks.

The hydrothermal method generally uses deionized water as the reaction medium, with hexadecylamine (HDA),[147–151] ethylenediamine (EDA),[152–154] octadecylamine (ODA)[155–157] and PVP[69,158,159] as the limiting ligand. By controlling the heating temperature, limiting ligand concentration and reaction time, CuNWs with different lengths and diameters can be obtained (Fig. 3a).[152] Conductive networks composed of copper nanowires can be used to prepare transparent conductive films owing to the low duty cycle.[50] Considering the superposition and entanglement of multiple nanowires in practical applications, such as transparent conductive films, it is often desirable to synthesize CuNWs with a small diameter and longer length. Zhong *et al.* synthesized well-dispersed CuNWs with an average diameter of 28 ± 2.7 nm and a length of several hundred microns by using HDA as the capping agent.[160] HDA is a limiting ligand widely that is used in the synthesis of copper nanowires. It can be used as a capping agent for the synthesis of copper nanowires, and can also be used as a ligand to enhance the dispersion of copper nanowires and reduce the agglomeration of the nanowires, as shown in Fig. 3b.[161] The diameter of CuNWs can be reduced by increasing the reaction temperature and ligand/reducing agent concentration. However, when the diameter is less than 30 nm, it is difficult for CuNWs to exist uniformly and stably due to the surface effect of the small-sized particl es.[148] Kim *et al.* first proposed the synthesis of ultrafine CuNWs with an average diameter of 11.3 nm and

Table 2 Summary of CuNWs inks detailing the materials, capping agents, reductant, length, diameter, figure of merit (FoM) and sheet resistance

| Material	Capping agent/reductant	Length (μm)	Diameter (nm)	FoM	Sheet resistance (Ω sq^{-1})	Ref.
Cu(NO$_3$)$_2$	EDA/hydrazine	10 ± 3	90 ± 10	52.3	15	152
CuCl$_2$	HDA/glucose	35	50	72.3	25	147
CuCl$_2$	HDA/glucose	5–100	44.6	119.0	24	148
CuCl$_2$	HDA/glucose	>50	66 ± 17	NA	NA	163
CuCl$_2$	HDA, PVP/glucose	>100	28 ± 2.7	117	9.5	160
CuCl$_2$	Oleylamine/ascorbic acid	41.2 ± 22	100 ± 47	192.6	10.3	164
CuCl$_2$	Oleylamine/tris(trimethylsilyl)silane	10–20	21 ± 4	89.8	35	60
CuCl$_2$	Oleylamine/ascorbic acid	41.2 ± 22	115 ± 5	107.2	12.6	165
CuCl$_2$/Cu(acac)2	Oleylamine/octadecene	35–45	30–35	41.2	24.5	77
CuCl$_2$	Oleylamine/ascorbic acid	40 ± 21	134 ± 4	177.7	7.6	166
CuCl$_2$	HDA/glucose	Aspect ratio	1570	110.9	46	161
CuCl$_2$	ODA/glucose	38 ± 2	62 ± 14	48.5	35	167
CuCl$_2$	HDA/WS$_2$	70	11.3	154.3	28.5	162
CuCl$_2$	HDA/glucose	49.3 ± 19.9	45.4 ± 17.4	66.8	31	168
CuCl$_2$	HDA/glucose	NA	40	93.4	60	169
CuCl$_2$	HDA/glucose	NA	30	111.3	19	170
CuCl$_2$	HDA/glucose	>100	36	80.9	34.05	171
CuCl$_2$	HDA/glucose	NA	NA	248.1	14.2	61
CuCl$_2$	ODA/glucose	20–50	30–90	79.8	20	155
CuCl$_2$	HDA/glucose	30 ± 13	36 ± 5	47.7	31.6	151
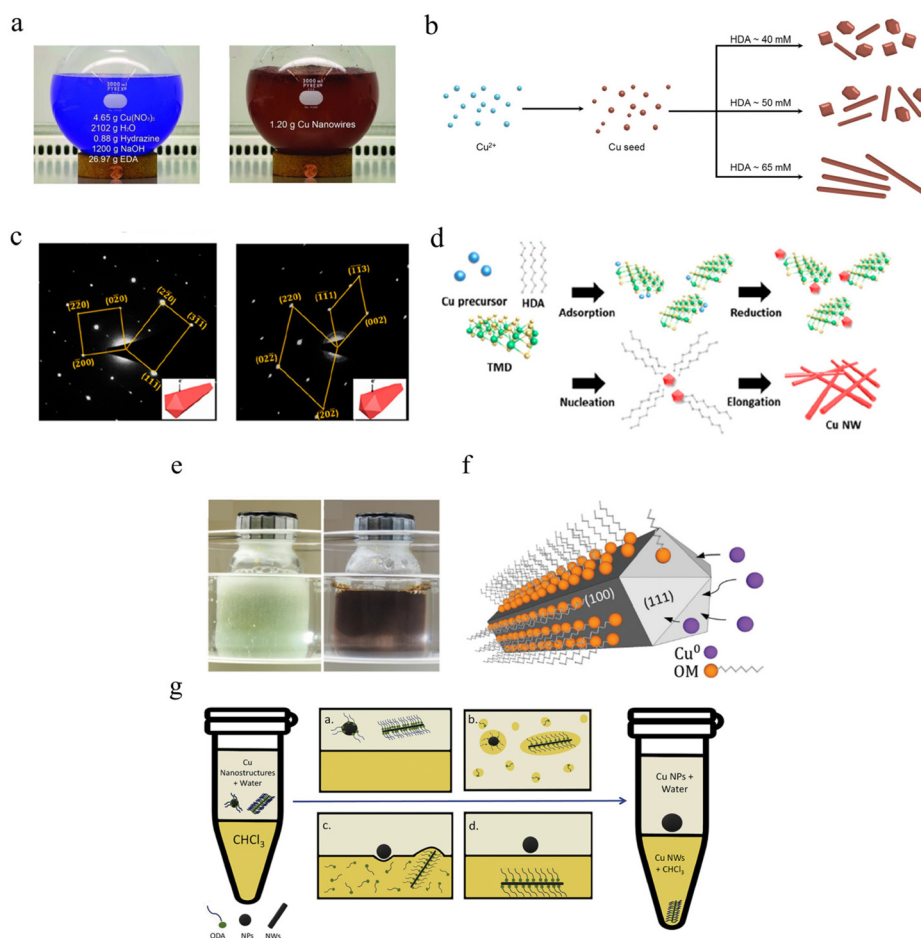
Fig. 3 Synthesis of CuNWs. (a) Optical image of the hydrothermal method.[152] Reproduced with permission from ref. 152. Copyright 2010 John Wiley and Sons. (b) Schematic image of the growth of CuNWs with different concentrations of HDA.[161] Reproduced with permission from ref. 161. Copyright 2020 Springer. (c) SAED pattern of CuNWs with the incident beam perpendicular/parallel to one of the side facets.[162] (d) Schematic illustration of the growth of CuNWs with WS₂.[162] Reproduced with permission from ref. 162. Copyright 2020 American Chemical Society. (e) Optical image of organic solvent methods.[164] (f) Schematic of the formation of CuNWs using OM.[164] Reproduced with permission from ref. 164. Copyright 2017 John Wiley and Sons. (g) Schematic diagram of the separation and purification CuNWs.[167] Reproduced with permission from ref. 167. Copyright 2020 Elsevier.

length of 70μm using tungsten disulfide nanosheets as the catalytic reducing agent, copper chloride as the copper source, and HDA as the limiting ligand.[162] As shown in Fig. 3c and d, HRTEM analysis showed that the CuNWs grew along the (110) direction, consistent with the conventional growth mode. This reveals the effectiveness of transition metal dichalcogenides (TMDs) in synthesizing metal nanowires.

The organic solvent method is similar to that of aqueous phase synthesis. Notably, the organic solvent can not only be used as a reaction site but also as a limiting ligand to control the uniaxial growth of CuNWs.[77,165,166] As shown in Fig. 3e, ascorbic acid (AA) was used as a reducing agent with oleylamine (OM) was the solvent and limiting ligand to guide the growth of CuNWs.[164] Elemental copper, as a face-centered cubic (FCC) structure, exhibits the highest atomic packing density in the (111) direction. Therefore, OM tends to adsorb on the (100) surface with stronger surface activity, resulting in

limited copper core growth in this direction, and finally guiding CuNWs to grow along the (110) direction (Fig. 3f). CuNWs are generally synthesized along with trace copper nanoparticles in the process, which can be effectively separated and purified by adding hydrophobic organic solvents. In addition, Hashimi et al. dispersed CuNWs in the organic phase by adding chloroform (CHCl₃) to achieve the effect of separation and purification from CuNPs, as shown in Fig. 3g.[167] The organic solvent residue needs to be removed by increasing the heating temperature. Meanwhile, excessive organic matter will affect the conductivity of the nanowires. Aqueous phase synthesis has the advantages of fast reaction, minimal residue, and convenient purification, which is widely used in experimental studies. Although CuNWs have excellent light transmittance and flexibility, electron scattering is intensified when the diameter is reduced to the mean free path of copper (40 nm), which usually makes the film produced by

CuNWs much less conductive than film produced from dense sintered copper film.

2.3. Copper precursor ink

Copper precursor inks can decompose to produce elemental copper under the action of reducing agents by heating or light irradiation, while the ligands evaporate in the gaseous state. The existence of Cu(II) gives the ink the specific characteristics of long stability and easy processing, which effectively avoids the oxidation and precipitation of copper in the storage period, and greatly improves the convenience of Cu ink.[127,172,173] Information on copper precursor inks in terms of the materials, reducing agents, sintering methods, and resistivity is listed in Table 3. Among previously reported Cu metal–organic decomposition (MOD) inks, copper formate ($Cu(HCOO)_2$) is regarded as an ideal precursor material owing to its advantages of good oxidation resistance in air, low thermal decomposition temperature (150–250 °C), low amounts of residue and low price.[174–176] Its decomposition equation is as follows: $Cu(HCOO)_2 \rightarrow Cu + H_2 + 2CO_2 + H_2O$. In order to improve the processing efficiency of copper precursor ink, an amine ligand was introduced to provide central copper ions with electron-induced partial reduction of copper(II), which significantly reduced the temperature required for copper reduction. Since coordination can be formed in all six directions of the Cu(II) space, the configuration of the Cu complex changes from octahedron to square plane during the reduction process, and finally metal Cu is obtained.[177] Kim et al. sintered copper foil with the lowest resistivity of 5.2 μΩ cm in a formic acid atmosphere by mixing copper formate and hexylamine, and pointed out that the content of hexamine affects the size distribution of copper particles (inverse ratio).[178] Choi et al. compared the effect of different concentrations of hexylamine on copper nucleation and found that higher concentrations resulted in the formation of small CuNPs and less porous copper films, as shown in Fig. 4a.[179] The role of hexylamine as a reducing and capping agent in the decomposition of copper precursor ink was confirmed, as shown in Fig. 4a. Compared with monoamine, diamine can be heated to produce imine, thus competing for O_2 molecules on the active site of the copper surface to improve

oxidation. Dong et al. used 1,2-diaminopropane (PDA) and copper formate as precursors and heated them directly in air to obtain a copper film with a resistivity of 18 μΩ cm.[172]

In the copper formate–amine complex, the decomposition temperature is determined by the interaction between hydrogen on the amine group and oxygen in the formate root (hydrogen bond); the size and porosity of the copper particles formed after sintering are also affected by the boiling point and coordination capacity of amine.[183,184] Paquet et al. used a variety of amines to coordinate copper formate, and found that the decomposition temperature of copper formate gradually increased with the increase of hydrogen bonding.[180] In addition, they also found that amines with a medium boiling point and strong coordination ability with the central copper ion (2-ethyl-1-hexylamine, octylamine and, decamine) can be sintered at low temperature to obtain good conductivity (140 °C, 7 μΩ cm), which is due to the rapid volatilization of amines with low boiling points and weak coordination ability during sintering, resulting in uneven growth size and agglomeration of the copper cores (Fig. 4b). In general, the decomposition of amine-coordinated copper formate can be divided into the processes of ligand decarboxylation and dehydrogenation to produce CO_2 and H_2. Shin et al. analyzed the key role of the amine ligand in dehydrogenation and dehydrogenation of copper formate from a theoretical perspective, and found that the hydride dimer of Cu(II) self-reduced to produce a stable binuclear Cu(I) compound after dehydrogenation (Fig. 4c).[181] Although Cu MOD ink is convenient, the low copper content in the solution results in relatively large resistance, and the generation of gas will also lead to pores in the film and affect the uniformity of film formation. In addition, CuO as a copper precursor ink can be used to improve the Cu content.[65,185,186] Rahman et al. prepared Cu patterns (resistivity ranged from 9.5 to 71.6 μΩ cm) from commercial CuO ink using a green laser (532 nm).[187] Rager et al. used CuO ink to prepare highly conductive Cu patterns (10 μΩ cm) on PET substrates; the CuO was reduced to Cu(0) under photonic radiation and grew into stable Cu patterns,[182] as shown in Fig. 4d, in which the decomposition needs suitable reductants or high-energy irradiation to produce Cu(0).

Table 3 Summary of Cu precursor inks detailing materials, reducing agent, substrate, printing methods, post-treatment methods and resistivity

| Material	Reducing agent/ligand	Substrate	Method	Post-treatment method	Resistivity (μΩ cm)	Ref.
Cu(II) formate	Hexylamine	Glass	Mayer coating	250 °C formic acid gas	5.2	178
Cu(II) formate	Hexylamine	Glass	Doctor-blading	200 °C formic acid gas	40.5	179
Cu(II) formate	AMP	Glass	Inkjet	190 °C N_2	10.5	177
Cu(II) formate	DPM	PI	Screen	IPL	NA	173
Cu(II) formate	PDA	PI	Spin-coating	180 °C in air	18	172
Cu(II) formate	Dipropylamine/3-butylpyridine	Glass	NA	95 °C in N_2	8	188
Cu(II) formate	2-Ethyl-1-hexylamine	PI	Doctor-blading	140 °C in N_2	7	180
Cu(II) formate	Pentylamine	Glass	NA	110 °C in N_2	5.7	175
Cu(II) sulfate	NaBH$_4$	PI	Inkjet	Electroless plating	5.68	189
Cu(II) nitrate	EG	PDMS	Spin-coating	Laser	90	190
Cu ion	Formic acid, acetic acid/ammonia–water	PI	Inkjet	IPL	2.3	191
CuO	NA	Paper	Inkjet	IPL	3.1	65
CuO	EG	PET	Inkjet	IPL	10	182
CuO	EG	Glass	Spin-coating	Laser	9.5	187
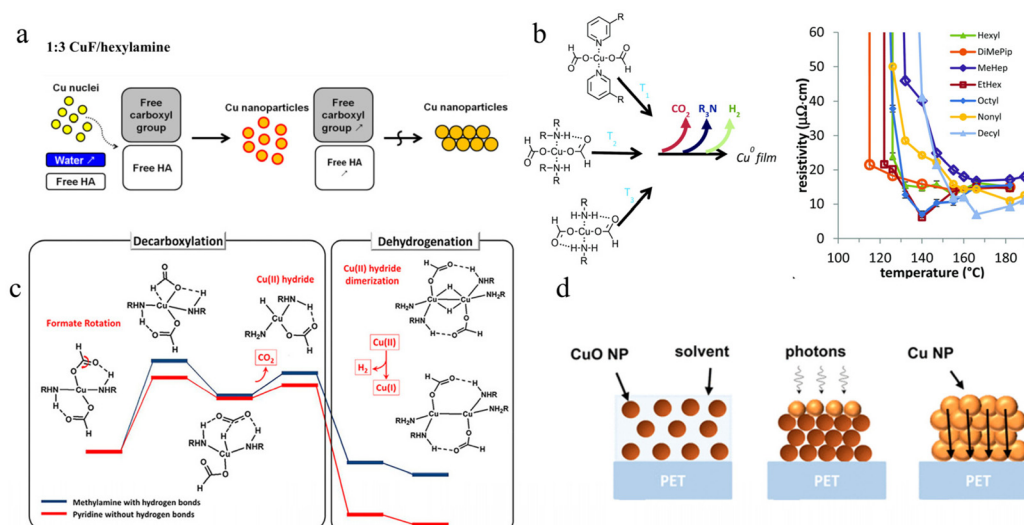
Fig. 4 (a) Mechanism of reaction of different concentrations of hexylamine to produce CuNPs.[179] Reproduced with permission from ref. 179. Copyright 2015 American Chemical Society. (b) Diagram of the decomposition temperature affected by hydrogen bonding of ligands ($T_1 < T_2 < T_3$) and the resistivity of films formed by sintering various complexes.[180] Reproduced with permission from ref. 180. Copyright 2018 Royal Society of Chemistry. (c) Schematic of the decomposition of copper formate with amine coordination.[181] Reproduced with permission from ref. 181. Copyright 2020 American Chemical Society. (d) Schematic of the decomposition from CuO to Cu.[182] Reproduced with permission from ref. 182. Copyright 2016 American Chemical Society.

2.4. Copper mixed ink

Copper films with uniform particle size and good connection between particles show higher conductivity and oxidation resistance. To improve the copper film quality, an extra conductive filler was added to the copper ink to increase the bridging property.[55,66,121,128,129,135,192,193] As the growth of copper particles is affected by temperature, pH, ligand, and other factors in the process of sintering of precursor ink, it is difficult to form a uniform microstructure. Li *et al.* proposed to add an appropriate amount of submicron copper 'seeds' into the copper–amino complex to provide heterogeneous nucleation sites for self-reduction of copper precursor.[132] In this method, a dense and thick copper conductive pattern with uniform microstructure and low resistivity (11.3 μΩ cm) was achieved, and the copper content in the ink was improved. Similarly, Jang *et al.* added CuNPs to the precursor ink of $Cu(NO_3)_2$ to improve the weldability between the particles, resulting in an electrode with a resistivity of 19.98 μΩ cm after flash sintering,[124] as shown in Fig. 5a. In addition, adding conductive metal nanowires into copper precursor ink can change the growth of the copper cores from homogeneous to heterogeneous,[125] which can control the growth of copper particles more closely arranged on the metal nanowire, resulting in the decomposition of copper precursors at low temperature (14.9 μΩ cm, sintering at 140 °C), as shown in Fig. 5b.

Compared with precursor ink, copper particle ink requires a higher sintering temperature due to the copper cores melting, so the main improvement strategy is to add a metal filler with a lower melting point to copper particle ink.[194] Chen *et al.* developed a copper–tin (Cu–Sn) mixed ink,[131] and

conductive copper film with sheet resistance of 14 Ω/sq was obtained by sintering metal nanoparticles with low photon energy. The excellent catalytic effect of copper can promote the self-reduction of other metal precursor inks, and the self-reduction nucleation of the filler metal can in turn promote the connection between the particles of copper ink after printing. Tomotoshi *et al.* took advantage of the catalytic effect of copper and added nickel formate and 1-amino-2-propanol complex (NiF-AMIP) into micron copper sheet to catalyze the *in situ* production of Ni at 150 °C in air to obtain a conductive film with a conductivity of 66 μΩ cm.[123] The addition of copper reduces the temperature of NiF self-reduction and provides a site for Ni nucleation. In turn, the Ni attached to the growth of copper nuclei can form necking connections between copper particles, thus achieving high conductivity and isolation of the contact between copper and external H_2O or O_2, and improving the long-term stability of the printed film (the resistance increases by 1.8 times in 7 days at 80 °C and 80% RH), as shown in Fig. 5c and d. This method can be also used to prepare nanoparticles with core–shell structure by using the catalytic formation of nickel by copper,[127] which showed excellent conductivity as low as 19 μΩ cm. In addition, CNT is also added to Cu ink to improve film uniformity.[130,173,195] However, the resistivity of CNTs is higher than that of pure copper, thus the resistance of sintered pattern is increased. Although mixed copper ink has great advantages, including increasing the copper content of ink, improved ink film conductivity, and lower porosity, and its convenient storage condition and simple preparation technology for large-scale application, some conductive fillers (such as silver or nanoscale precious metals)
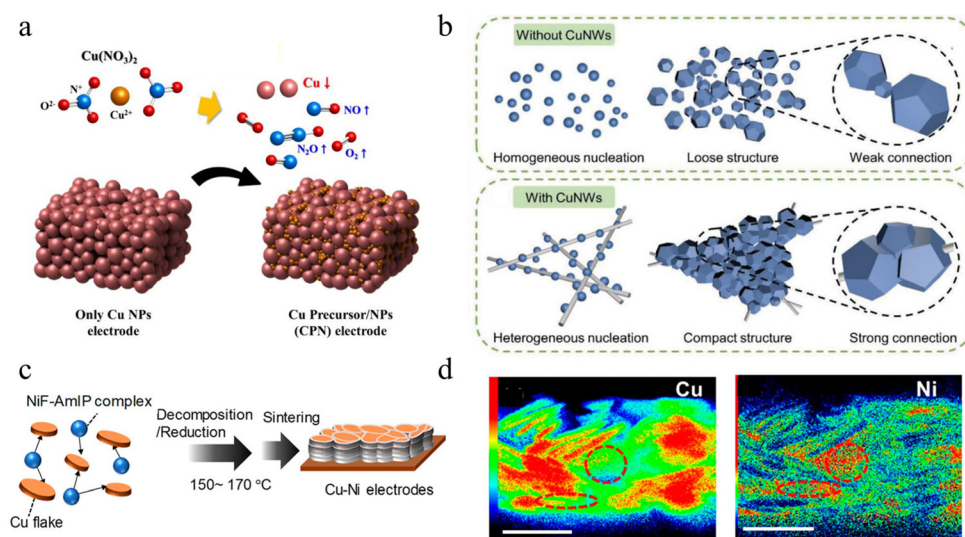
Fig. 5 (a) Schematic of adding CuNPs to $Cu(NO_3)_2$ for improving formation quality.[124] Reproduced with permission from ref. 124. Copyright 2021 Springer. (b) Schematic of metal nanowires providing nucleation sites for CuNPs growth.[125] Reproduced with permission from ref. 125. Copyright 2019 John Wiley and Sons. (c) Schematic of the decomposition/reduction of NiF–AmIP complex with Cu.[123] (d) Cross-sectional elemental distribution maps of Cu and Ni.[123] Reproduced with permission from ref. 123. Copyright 2021 American Chemical Society.

are expensive, which is inconsistent with the starting point of the low price of copper.

3. Printing and sintering methods

Conventional processes (photolithography,[196,197] vacuum deposition,[198] etching,[199] *etc.*) have high requirements for equipment and harsh preparation conditions, which limit the application and large-scale preparation of electronic devices on different substrates, and cause more waste. Conductive ink adopts the additive manufacturing method because of its special rheological properties, which can be utilized to produce flexible and robust electronic devices on a variety of

substrates through printing techniques.[200–203] For the process of printing of electronic devices, the goal is to obtain qualified components or working circuits. Therefore, it is necessary to regulate the performance of ink according to the printing mode. For copper-based ink, the parameters to be controlled are viscosity, surface tension, copper content and particle size. The first two parameters limit the printing mode of the ink, while the latter two parameters affect the quality of the printed copper film. In this section, we will first introduce some printing processes applicable to copper-based ink and the basic requirements of this process for ink; the related information can be viewed in Table 4.[71,117,142,207,218] Then we will introduce various methods for sintering; the related information can be viewed in Table 5.[94,123,252,263,266]

Table 4 Summary of printing processes

Printing process	Principle	Advantages	Drawbacks	Line width (μm)	Printing speed	Viscosity (cP)
Inkjet printing	Extrusion of droplets by piezoelectric deformation or thermal expansion	Low wastage of inks; good smoothness of ink trace; good operability	Clogging of nozzles; coffee-ring effect; satellite points; low adhesion	>10	Moderate	1–20
Direct writing	Extrusion of inks through air pressure	Convenient operation; wide range of ink applications	Ink clogging causes printing discontinuity; high requirements for ink rheological performance	>500	Moderate	10^2–10^6
EHD jet printing	Pull the inks by electric field force	Flexible operation; high printing efficiency; wide suitability of inks	Expensive instruments; complex operation	>0.1	Low	1–10^4
Screen printing	Transfer ink from a screen plate to a substrate by scraper	Rapid large-scale production; easy operation; low-cost instruments	High roughness of ink trace; higher viscosity ink required	>30	High	>500

Table 5 Summary of sintering processes

Sintering process	Principle	Advantages	Drawbacks	Operating conditions	Sintering speed
IPL sintering	Decomposition of organic capping agents and necking of copper particles due to light radiation	Convenient operation; quick completion; large scale; wide range of ink applications	Low resolution; concentrated energy in a short time	Ambient conditions	<10 ms
Laser sintering	Generating a hot spot in a very small area to achieve welding	Flexible operation; pattering [A51]	Expensive instruments; low sintering depth; low efficiency	Ambient conditions	<100 μs for each spot
Plasma sintering	Removal of organic matter using high-energy ions and electrons	Mild sintering temperature; flexible substrates can be stabilized	Expensive instruments; low efficiency; complex operating conditions	Vacuum or low-pressure conditions	>10 min
Thermal sintering	Thermal decomposition of organic matter and reduction of copper oxide	Convenient operation; inexpensive instruments	High temperature destroys flexible substrate; oxidation is prone to occur; high porosity	Vacuum or inert gas conditions	10–30 min
Chemical sintering	Reduction of acidic solutions	Simple operation; room-temperature processing; short time	Additional cleaning process; pollution; insignificant sintering effect	Ambient conditions	<1 min

3.1. Printing conductive Cu ink

3.1.1. Inkjet printing. As a digital printing method, inkjet printing is widely used in the electronic manufacturing industry for its wide applicability and convenience.[204–208] The method of drop-on-demand (DOD) inkjet printing is often used to prevent pollution and waste of Cu ink, as shown in Fig. 6a.[209] The ink performance requirements for inkjet printing are mainly reflected in viscosity and surface tension. Derby *et al.* found that good inkjet printing can be achieved when the reciprocal of Oh is in the range of (1,10),[210] so printable inks generally require suitable viscosity and surface tension. Oh is defined as:

$$\text{Oh} = \frac{\sqrt{\text{We}}}{Re} = \frac{\eta}{\sqrt{\gamma \rho l}}$$

where η, ρ, γ, and l represent the viscosity, density and surface tension of the fluid, respectively, and l is the diameter of the nozzle.

The dispersion stability of copper particles in ink is one of the key factors affecting whether the ink can be ejected from the nozzle. Excessive particle size and agglomeration between particles will block the nozzle. To achieve good printing ability, the size of copper particles should normally be less than a hundredth of the size of the nozzle diameter.[142] Therefore, copper particles with large size or length are usually screened out through a filter before printing. To avoid nozzle clogging, Kim *et al.* reported a method for preparing conductive copper patterns by inkjet printing of copper sulfate and sodium phosphinate inks.[206] Although inkjet printing has
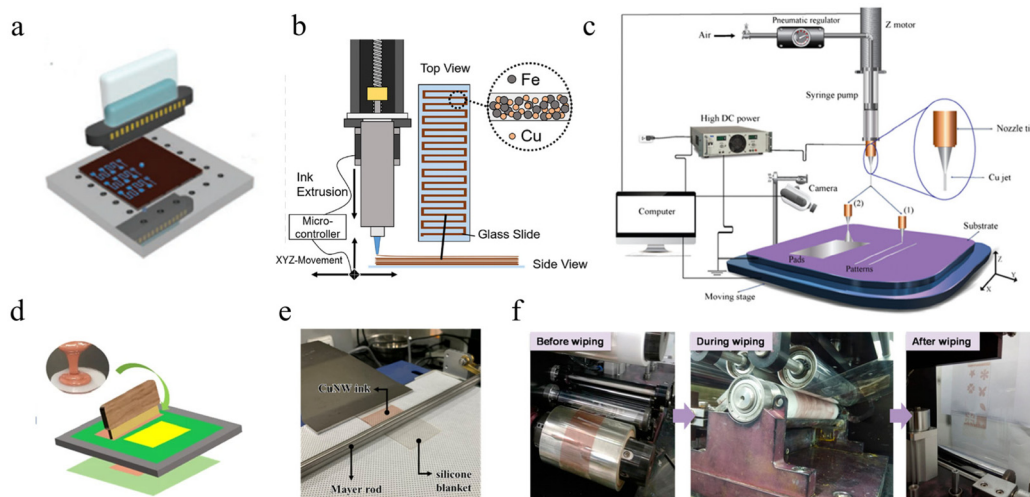

Fig. 6 Printing methods for Cu inks. (a) Schematic of inkjet printing for CuNPs.[209] Reproduced with permission from ref. 209. Copyright 2019 John Wiley and Sons. (b) Schematic of the fabrication of Cu–Fe mixed ink by direct writing.[211] Reproduced with permission from ref. 211. Copyright 2020 Elsevier. (c) Schematic diagram showing EHD jet printing.[117] Reproduced with permission from ref. 117. Copyright 2019 John Wiley and Sons. (d) Schematic illustration of screen printing.[112] Reproduced with permission from ref. 112. Copyright 2022 Springer. (e) Optical image of Mayer rod for printing CuNWs ink.[151] Reproduced with permission from ref. 151. Copyright 2022 American Chemical Society. (f) Optical image of large-scale R2R printing.[212] Reproduced with permission from ref. 212. Copyright 2016 American Chemical Society.

good operability and high resolution, owing to the low viscosity of the ink, the adhesion of the printed pattern to the substrate is a major problem. Moreover, the diffusion behavior of the ink on the substrate can also lead to the phenomenon of edge burrs and coffeering.[208] To overcome this problem, an efficient route is modifying the printing substrate with a nanostructured self-assembly layer with 3-mercaptopropyltrimethoxysilane,[191] which forms a silanol bond with the oxygen-treated PI film. The functional group on the other side forms a Cu–S bond with copper, which significantly enhances the adhesion of inkjet printing copper on PI. In addition, increasing the contact angle between the copper ink and the substrate can also increase the control of the printing pattern and reduce the disorder diffusion at the edge of the printed ink. Jun *et al.* pretreated the Si/SiO$_2$ substrate with hexamethyldisilazane (HMDS), improved the contact angle of inkjet printing copper ink, and obtained a printing pattern with regular edges and no coffee-ring phenomenon.[116] However, due to the entanglement of nanowires, there are few applications in inkjet printing.[213–215]

3.1.2. Direct writing. Direct writing extrudes the liquid in the jet cavity out of the nozzle through air pressure to form a continuous cylindrical ink mark. As a subset of 3D printing, direct ink writing requires the ink to have the characteristics of viscoelasticity, shear thinning, and yield stress flow. Therefore, the printable ink range of direct ink writing is wider, being able to print both copper particles and nanowire ink.[216] Siebert *et al.* prepared an acetone gas sensor that can work at high temperature by writing copper and iron mixed ink on a glass substrate in direct writing, and realized nanotip conduction between copper and iron and their oxides.[211] Khuje *et al.* also demonstrated direct writing of CuNWs ink on flexible ceramics to prepare pressure sensors.[217] The viscosity of the ink usually leads to the cylinder ink diameter (D) that is extruded from the nozzle being larger than the nozzle diameter (d). Considering the height of the nozzle (H) from the substrate and the ink outflow speed (V) from the nozzle, ideally, due to the conservation of volume, the initial ink diameter printed on the substrate will be $l = D\sqrt{\frac{V}{C}}$, where C is the moving speed of the nozzle relative to the substrate.[218] Owing to the existence of the forward contact angle, the line width will be slightly higher than l, so an effective way to improve the resolution is to increase the nozzle movement rate to close to the ink outflow rate or higher.

3.1.3. Electrohydrodynamic jet printing. Electrohydrodynamic (EHD) jet printing differs from the traditional way of extruding ink by mechanical force. Its principle is to pull the ink out of the nozzle by electric field force,[219–222] as shown in Fig. 6c. When applying the high-voltage electric field between the nozzle and the substrate, the conductive ink in the spray chamber forms conical droplets (Taylor cone) at the nozzle through the movement of charge. At this time, the ink's electric field force and gravity in the cone balance the viscosity and surface tension of the ink. If a positive voltage pulse is applied, the balance will be destroyed, resulting in a very fine droplet flow from the tip of the Taylor cone, which is finally printed on the substrate. By controlling the relationship between the electric field force, ink viscosity, and surface tension, EHD jet printing can realize four printing modes: point spraying, surface spraying, line spraying, and whip writing.[223] EHD jet printing has the characteristics of flexible operation, high printing efficiency, and a wide range of ink viscosity. Inks that are suitable for inkjet and 3D printing can be applied for EHD jet printing. The most significant advantage is that the size of the printing ink is far smaller than the nozzle diameter, which gives EHD jet printing great advantages in micro preparation, such as for thin-film transistors and integrated circuits. Can *et al.* stably printed copper electrodes with a 40 μm line width at 8000 μm s^{-1} by deposition of high-viscosity copper ink (4000 cPs) on ZTO using EHD jet printing technology.[117] High-viscosity ink made the lines less diffused, the edges were neat, and the pattern fidelity was high after printing.

3.1.4. Screen printing. Screen printing uses a scraper to transfer ink from a screen plate to a substrate.[224–227] As a plate printing method, screen printing can achieve rapid large-scale production. The ink floats on top of the patterned screen at rest and is printed on the substrate through the mesh after receiving a shear force. This requires a high-viscosity ink. Therefore, ink with a high filler content, such as copper particle ink and copper mixed ink, is usually used. The printed ink layer is thick (tens of microns) and has good adhesion to the substrate.[225,228] However, the disadvantages are the high roughness of the deposited film and the low resolution. It is usually used to prepare passive devices, such as electrodes or antenna,[98,112,114,121,127,229] as shown in Fig. 6d.

3.1.5. Other printing techniques. Gravure printing and flexographic printing press ink onto the substrate by customizing the patterns on the roller.[230–232] In this way, high-quality patterns can be obtained quickly and can be combined with the roll-to-roll (R2R) printing process to complete coating, patterning, and packaging to obtain devices. Zhong *et al.* added a roller with an isopropanol (IPA) soaked towel to the R2R to selectively erase the unsintered CuNWs pattern at a speed of ~2 m min^{-1}, as shown in Fig. 6f. There is little difference between the sheet resistance (R_s) before (17.8 ± 1.8 Ω sq^{-1}) and after wiping (17.4 ± 1.8 Ω sq^{-1}), and there is no significant change in the bending radius range of 1.5–24 mm.[212] There is no doubt that R2R printing is the best solution to achieve large-scale and rapid production, which is also in line with the price advantage of copper itself.

Similarly, Mayer rod coating uses gaps in the wire coiled around the bar to scrape off the excess solution,[171,233,234] as shown in Fig. 6e. This technique can effectively control the thickness of the coating (about 1/10 of the wire diameter) and has a small footprint for direct application to R2R processes. Compared to screen and gravure printing, the ink has a lower additive content, so the resulting film performs better in terms of electrical conductivity.[13,235]

Printing resolution and printing rate have an inverse relationship. In general, to achieve high-resolution printing, non-contact digital printing techniques such as inkjet printing and EHD printing are good choices. They avoid direct contact

with the substrate during printing, ensure the completeness of the ink, and achieve high precision printing. However, micro-processing manufacturing the printing rate slower and the cost of equipment is higher. Screen printing, gravure printing, spray-coating, and other non-digital printing methods can be done at high speed using a mask, but the disadvantage is that it is difficult to achieve high-resolution manufacturing (<10 μm). Recently, Kim et al. reported a reverse-offset printing technology,[151] in which CuNWs were coated by Mayer rod and then transferred to a gravure plate. They used a commercial adhesive hand-roller to achieve the directional transfer of patterned ink to obtain CuNW patterns with a minimum line width of 7 μm. This printing method provides a potential solution for the rapid and efficient preparation of copper-based inks. To achieve high throughput and quality functional components, combining multiple printing methods may be an effective way to break the conflict between resolution and printing rate.

3.2. Sintering treatment methods

The preparation of conductive copper inks usually requires the addition of organic ligands such as capping agents and dispersants to improve the oxidation resistance and dispersibility of the ink. For conductivity, the covalent bonds between these fillers can restrict electron transfer and reduce film uniformity. Moreover, the high specific surface area of CuNPs will inevitably oxidize during preparation. Thus, it is necessary to employ an additional sintering process to remove these fillers to connect bare copper particles to achieve conductivity. There is an additional reductive decomposition process for copper precursors or copper mixed inks to guide the nucleation growth of copper or other conductive metal fillers.[72] The quality of the sintered film can usually be measured in three aspects: (a) the degree of bridging between copper particles; (b) the porosity of the copper film; (c) the amount of oxide (CuO, Cu_2O) and organic residue content. The more uniform the necking connection between copper particles, the smaller the film's porosity and the lower the amount of residue, which significantly improves the electrical conductivity of the sintered copper film. In order to improve the electrical properties of printed copper inks, various sintering processes have been developed, including photonic sintering, intense pulsed light (IPL) sintering, laser sintering, plasma sintering, thermal sintering, and chemical sintering.

3.2.1. Photonic sintering.
Photonic sintering uses light radiation energy to complete the sintering of copper inks. The printed ink layer absorbs specific wavelengths of light irradiation to generate enough heat to decompose organic residues, while the extremely low melting point of nano-sized copper (100–300 °C) can achieve local melting and interconnection.[240,241] Conversely, the flexible substrate absorbs few incident waves so it will not be destroyed. When sintering different copper inks, it is necessary to consider the wavelength to match the absorption spectrum of the material, Fig. 7a shows a xenon lamp combined with NIR and deep UV lamp to achieve all-photonic drying and sintering of the Cu

ink.[236] Copper precursor inks exhibit high absorption peaks below 400 nm and are often sintered by UV.[242] UV sintering can yield conductive patterns in a relatively short time, but the high-energy irradiation may make the decomposition process violent and produce large amounts of gas, resulting in uneven copper nucleation, excessive pores, and other factors. Although the absorption band of copper nanomaterials in the infrared region is small, infrared light has a strong thermal effect, which can quickly increase the temperature of the printed ink to achieve the decomposition of organics and thermal fusion of copper particles.[243] However, compared to UV sintering, IR sintering requires a longer time, which can lead to the oxidation of the copper part during the sintering process, affecting the pattern's conductivity.

3.2.2. Intense pulsed light sintering.
IPL sintering combines the advantages of UV sintering and IR sintering. It uses a broad-spectrum (200–1200 nm) xenon lamp to irradiate printed ink, which enables fast sintering within milliseconds in an air environment,[126,244–246] as shown in Fig. 7b. Meanwhile, the number of xenon lamps can be increased to achieve large-area sintering, making IPL sintering the most effective sintering method for achieving large-scale preparation of printed copper inks. The broad spectrum of IPL is usually able to be absorbed by any copper-containing materials (pure copper – visible band, copper precursor – UV band, CuO – 1033 nm, Cu_2O – 590 nm),[247,248] thus when irradiated by light, a variety of copper-containing composition absorb photon energy to be reduced to pure copper, improving the denseness of copper in printed films after sintering. However, the high energy of IPL in a short period may destroy some flexible substrates (PET, PEN) with low glass transition temperatures (T_g). Three optimization schemes are commonly used: (a) adding reducing ligands; (b) pre-drying; and (c) multiple pulses and optimized duty cycle. Zareei et al. used IPL to sinter copper–silver hybrid inks, and they found that adding ethylene glycol (EG) to the ink could reduce copper oxide on the surface of copper particles under the effect of high-temperature photothermal chemistry.[121] This phenomenon is attributed to the dehydration of EG to generate acetaldehyde.[249] Some other organic fillers were also found to have similar effects, such as PVP[54,237,250] and hexadecylamine (HDA),[246] as shown in Fig. 7c. Pre-drying the ink before IPL sintering can reduce the content of organic solvents in the marks, which prevents the rapid boiling and evaporation of solvents inside the film during IPL sintering.[121] For substrates with low T_g and thermal conductivity, using multi-pulse IPL sintering with the same energy density can effectively prevent a rapid increase in temperature.[94,115,244,245] Copper particle ink printed on paper substrate using a fixed energy density of 15.6 J cm^{-2} and three pulses of IPL with 80% duty cycle within 2 ms exhibited a resistivity of 2.8×10^{-7} Ω m.[94] In addition, Chu et al. obtained conductive films with low resistance (5.12 μΩ cm) by sintering copper–silver hybrid inks on PI substrates using an energy density of 7 J cm^{-2}, pulse time of 1 ms, off time of 9 ms, and 20 pulses.[129] Recently, Lee et al. developed a bidirectional IPL (B-IPL) sintering method that maintains uniform heating of the system by simultaneously radiating photon energy from
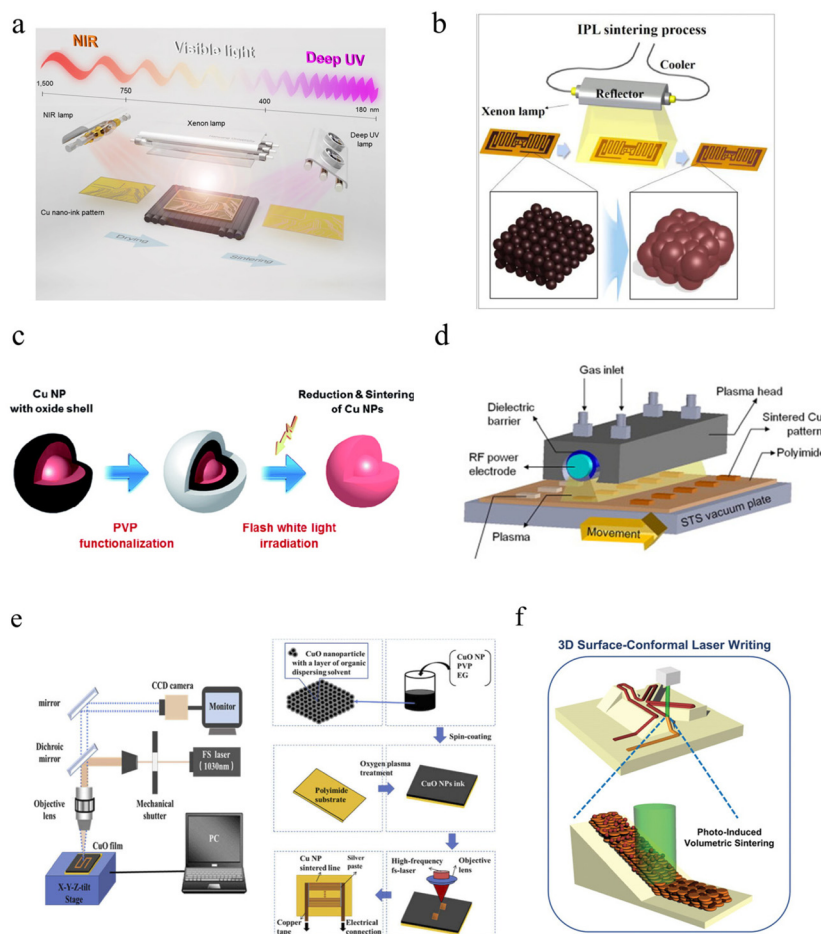
Fig. 7 Sintering methods for Cu inks. (a) Schematic of photonic drying and sintering of Cu ink.[236] Reproduced with permission from ref. 236. Copyright 2016 Springer. (b) Schematic image of IPL sintering.[126] Reproduced with permission from ref. 126. Copyright 2020 Elsevier. (c) Schematic of reactive sintering using IPL.[237] Reproduced with permission from ref. 237. Copyright 2017 Royal Society of Chemistry. (d) Schematic diagram of atmospheric-pressure plasma sintering system.[238] Reproduced with permission from ref. 238. Copyright 2013 Elsevier. (e) Schematic of laser and experiment flow for fabrication of a flexible circuit.[185] Reproduced with permission from ref. 185. Copyright 2021 Optical Society of America. (f) Schematic image of the 3D surface-conformal laser writing process for fabricating a copper circuit.[239] Reproduced with permission from ref. 239. Copyright 2020 John Wiley and Sons.

both front and back sides, avoiding the layering and empty cavities caused by local heat conduction inside the copper film by single-way pulsed light sintering.[114] IPL can achieve sintering effects not only on large areas, but also by introducing a mask to achieve specific patterning. It should be noted that the introduction of the mask causes the diffraction of light in the gap, resulting in a change in the line width of the sintering pattern. This is related to the excitation voltage of the xenon lamp.[212] Thus, IPL sintering requires the optimization of various parameters to achieve the best results when dealing with specific structures, which makes the sintering process tedious.

3.2.3. Laser sintering. Laser sintering focuses high-energy beams in petite sizes (micron scale) by emitting coherent light, and the sintering of copper ink in air can be achieved by selecting a laser of matching wavelength.[187,249,251–253] The principle of the laser sintering device is shown in Fig. 7e. The coherent light passes through a beam splitter and then passes through a microscopic objective to obtain a focused spot, the

size of which can be observed using the CCD above. The XYZ motion stage can be moved to achieve directional sintering of the printed ink marks. Huang *et al.* used a femtosecond laser to sinter CuO inks at 1030 nm.[185] High-resolution copper tracks with a resistivity of 130.9 μΩ cm and line width as small as 5.5 μm were obtained on PI substrates. The mechanism of CuO reduction can be explained by the dehydration decomposition of ethylene glycol in the ink to produce acetaldehyde, which was mentioned in the previous section. Laser sintering can be used for selective sintering of copper nanowire junctions. Han *et al.* used a 532 nm laser to sinter a percolation CuNWs network.[252] The laser-induced plasma effect on the metal surface at this wavelength enables localized welding at the nanowire junctions, which significantly reduces the contact resistance between nanowires. Most importantly, laser sintering can move along any structural surface, which gives the sintering digital properties with the potential for achieving three-dimensional structures and expanding the patterning of

printed films. However, it is usually poorly adapted to high-viscosity copper inks due to the low penetration depth.[254,255] FDTD simulations and experimental tests revealed that copper nanoparticles could reduce the plasmonic absorption of metal NPs and enhance the scattering effect when agglomerated around a copper micron sheet,[239] thus increasing the penetration depth of laser can achieve good sintering of printed copper ink of 16.5 μm thickness. A highly conductive copper film (15 μΩ cm) was formed on a 3D structure after laser irradiation with 532 nm wavelength. Laser sintering has shown great advantages in microfabrication, processing, and digitization. However, the sintering rate is too slow and it is difficult to further reduce the size of the focused spot due to the optical diffraction limit. Although it has been found that the introduction of microspheres under a microscope can significantly reduce the focused spot to break the physical limit, the reduction to micron-sized focal length poses a challenge to the processing method.[256–258]

3.2.4. Plasma sintering. Plasma sintering excites gases (Ar, H_2, O_2) to generate high-energy ions and electrons.[259–261] In the plasma system, the excited non-equilibrium species bombard the surface of the printed material with high electric potential energy (1–10 eV),[70] effectively removing organic matter from the copper ink, thermally decomposing precursors to produce copper nuclei, and promoting the diffusion of bare copper grain boundaries to achieve sintering; the equipment is shown in Fig. 7d. The greatest advantage of plasma sintering is the room-temperature operating environment, thus enabling sintering of printed patterns on flexible substrates (PEN, PET, etc.) at lower temperatures (~80 °C). The plasma has different chemical properties depending on the type of gas added to the cavity. Kim et al. used step-by-step plasma to sinter CuNP ink at 250 W to obtain films with a resistivity of 21.06 μΩ cm.[262] The organic phase was first decomposed by oxygen plasma in the presence of Ar, and hydrogen plasma was subsequently added to reduce the copper. This method is more efficient than sintering in a 350 °C calciner and protects the flexible substrate from high-temperature damage. Gao et al. prepared submicron copper particle ink on PET by sintering in a reverse particle etching (RIE) plasma sintering system using a mixture of H_2 and Ar.[238] Copper patterns with a resistivity of 15.9 μΩ cm were obtained by sintering for 10 min in an operating environment below 75 °C. Plasma sintering can also be used to treat copper precursor inks. Farraj et al. printed copper–AMP (2-amino-2-methyl-1-propanol) metal–organic decomposition (MOD) ink on PEN, and then used plasma with Ar and N_2 to sinter.[263] Highly conductive patterns with resistivity only four times that of pure copper (7.3 μΩ cm) were obtained after optimization of parameters such as pre-drying temperature, time, and amount of additives. However, the biggest disadvantage of plasma sintering is that the equipment is expensive, and most of it needs to be performed under vacuum and low pressure, which makes it challenging to apply to R2R printing. In addition, plasma has a limited penetration depth, which requires long sintering times (~10 minutes) and is less efficient.

3.2.5. Thermal sintering. Thermal sintering, as one of the most basic sintering methods, is widely used for the sintering of various copper inks for its convenience, ease of operation, and inexpensive equipment. Thermal sintering is achieved by directly raising the system's temperature to achieve the decomposition of the organic phase in the copper ink and mutual fusion between the particles. Although the melting point of bulk copper is as high as 1083.4 °C, it can be reduced to less than 300 °C as the particle size is reduced to the nanometer level.[240] Thus, copper inks can be sintered by instruments such as ovens, hot tables, and calciners.[74,113,122,123,150,264] However, the high decomposition temperature of the organic additives (e.g., PVP ~200 °C)[43,91] makes the sintering system destroy flexible substrates (PET, PEN, paper, fabric, etc.). Moreover, copper will produce oxides in an air atmosphere above 200 °C, so it is usually necessary to carry out the sintering under vacuum or inert gas.

3.2.6. Chemical sintering. Chemical sintering is more moderate than all the previous sintering methods and usually uses acidic solutions (formic acid,[265] acetic acid,[155,169] lactic acid,[266] etc.) to remove oxides and residues. Formic acid vapor has been used in both pretreatment and heat treatment processes.[265] The pretreatment with formic acid vapor replaced the organic protective layer around the copper nanoparticles to form easily decomposable copper formate, then ensured that the copper was not oxidized and a conductive network with conductivity of 9.1×10^4 S cm^{-1} (16% of that of bare copper) was obtained after the sintering process. In addition, Zhang et al. used lactic acid on sprayed CuNWs to remove organic coverings and oxides from the nanowire surface to reduce the contact resistance at CuNWs junctions.[266] Optimization experiments were performed to obtain the minimum resistance values using the parameters of 1 wt% concentration of lactic acid submerged for 5 min and seven sprayed layers. Chemical sintering has the advantages of simple operation, mild reaction conditions, and room-temperature processing, but the introduction of solutions can cause some pollution. At the same time, the printed copper films usually require an additional cleaning process to remove the residual solution, which may make the final film less conductive.

4. Antioxidant method

Owing to its atomic structure, copper can easily react with water and oxygen to produce oxides (CuO, Cu_2O) under ambient conditions.[267] Especially when the size is reduced to the nanometer level, the higher specific surface area will make copper more susceptible to oxidation, which will seriously hinder electron transfer and increase the resistance of the printed film. In addition, high melting point oxides (CuO ~1446 °C, Cu_2O ~1235 °C) can lead to holes and cracks inside the film during sintering, making the film highly porous and mechanically tough, which limits the application of printed copper inks in electronics.[45,142] Therefore, it is crucial to improve the stability of copper nanoparticles under environ-

mental conditions by introducing additional fillers and processes. Depending on the principle, there are two types: chemical and physical treatment.

4.1. Chemical treatment

Chemical protection usually uses a solvent to produce a protective layer or remove oxides from the copper. The most mainstream method is to produce a dense passivation layer consisting of metal salts on the outermost surface by reacting an organic corrosion inhibitor with the copper.[112,268,269] The passivation layer keeps O molecules from the environment and the electrochemical process of the doped material in the passivation layer can give the passivation layer resistance to acids and alkali. The commonly used corrosion inhibitors are azole nitrogen, amines and some self-assembled organic short chains.[270,271] Polat Genlik *et al.* used benzotriazole (BTA) to passivate the CuNW network. Surprisingly, they found that the sheet resistance of the BTA-passivated film increased by only 1 Ω sq^{-1} and the transmission decreased by only 2%.[168] After bonding with a PEDOT:PSS (pH < 4) layer, the transparent conductive film was not oxidized after heating at 150 °C, which allows the stable presence of CuNW flexible transparent electrodes during the preparation of optoelectronic devices. BTA can form a thin polymer layer that is insoluble in water and organic solvents on the surface of CuNWs, preventing the contact of Cu with O_2 and H_2O. Considering the toxicity of BTA, Zhou *et al.* investigated the passivation effect of 1,2,4-triazole with TT-LYK on the copper surface,[272] as shown in Fig. 8a. Both corrosion inhibitors can form coordination effects with copper surfaces to produce copper salts, and their reaction equations are shown below:

$$Cu^{2+} + 1,2,4\text{-triazole} \rightarrow Cu\text{-}1,2,4\text{-triazole}$$

$$Cu^{2+} + TT\text{-}LYK \rightarrow Cu\text{-}TT\text{-}LYK$$
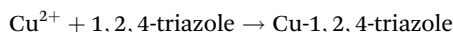
Using Freundlich adsorption isotherm fitting, the standard adsorption free energies of 1,2,4-triazole and TT-LYK were −25.92 kJ mol^{-1} and −23.43 kJ mol^{-1} (between −20 and 40 kJ mol^{-1}), respectively, indicating that these two corrosion inhibitors formed multiple passivation layers on the copper surface, mainly by physical adsorption and supplemented by chemical adsorption (Fig. 8b). The similarity of the two corrosion inhibitors in the adsorption type and passivation process allowed the mixture to improve the corrosion inhibition of the films further. Kwon *et al.* used 3-mercaptopropyl-trimethoxysilane (MPTS) to passivate the sintered copper films based on the strong covalent bonding between Cu and S.[191] The weak Cu(II) and Cu(I) elements present in the copper films were effectively removed to obtain the metal salt of $Cu(SC_3H_6Si(OCH_3)_3)$. This passivation layer protects the copper from resistance setting under ambient conditions for 15 days, as shown in Fig. 8c.

Self-assembled organic short chains play a prominent role in passivating copper without affecting the electrical conductivity. Recently, Peng *et al.* investigated the effect of passivating copper with sodium formate on oxidation resistance and corrosion without affecting electrical conductivity.[273] They found that the formate treatment leads to a (110) lattice reconstruction on the surface of copper foil. The four OH$^-$ on the double-core $Cu_2(\mu\text{-HCOO})_2(OH)_4$ match perfectly with the outermost Cu(II) to form a Cu(II) → Cu(I) → Cu(0) longitudinal structure. This dense passivation structure hinders the adsorption of oxygen and water on the copper surface and shows a good anticorrosion effect under the action of NaOH, salt spray, H_2O_2, and Na_2S, while the reason for not affecting the electrical conductivity may be the quantum tunneling effect. However, it should be noted that the formic acid passivation layer cannot exist under strongly acidic conditions, so the passivation process should avoid pH < 3. Based on the excellent effect of formate, Sheng *et al.* used iodine ions to control copper growth to obtain 2D morphological Cu nanoplates with (111) surface as the base.[97] The Cu nanoplates immersed in formate solution formed a dense passivation layer covered by formate on the Cu (111) surface after 12 h treatment at 120 °C. The passivated Cu-FA showed good stability at 350 °C and the resistance increased by only 10% after one day of immersion in 0.1 M NaOH solution (Fig. 8d). The formate decomposition temperature is low, with few by-product residues and good passivation protection, but the current studies all require a long treatment time (about 12 hours) in an formate solution environment to obtain good passivation.

In addition, the use of acidic solutions (lactic acid, acetic acid, formic acid) also plays a role in improving the electrical conductivity.[173,265,275] The reason is that acids can remove oxides from the surface of copper particles through reduction reactions, and most organic capping agents (such as HDA and ODA) are more soluble in acidic solvents. Therefore, acids can be used to remove oxide and organic residues during the deposition of CuNWs for transparent conductive films. Hashimi *et al.* prepared transparent films of CuNWs with a sheet resistance of 35 Ω sq^{-1} and 81% transmittance using an optimized purification method.[167] Owing to the oxidation problem of copper nanowires with a high aspect ratio, the sheet resistance initially increased 10 times. However, the sheet resistance of the film can be significantly reduced to the initial value by acetic acid immersion for 10 min, and this phenomenon can be repeated up to five times. Acid solvent immersion treatment is simple and fast, but can cause environmental pollution problems, while an excessive number of rinses will reduce the initial conductivity of copper printed films, which is caused by the peeling of copper particles from the surface during the cleaning process (Fig. 8e).

4.2. Physical treatment

Physical protection also involves applying a protective layer, but the difference is that no chemical reaction is involved in the formation of copper salts. Depending on the degree of encapsulation, physical protection can be divided into core–shell and coating structures.

4.2.1. The core–shell structure.
The core–shell structure provides protection by forming a perfectly encapsulated antioxidant shell layer on the outside. The shell layer material can be inorganic oxides (SiO_2, Al_2O_3, ZnO),[276,277] metals (Ag, Au,
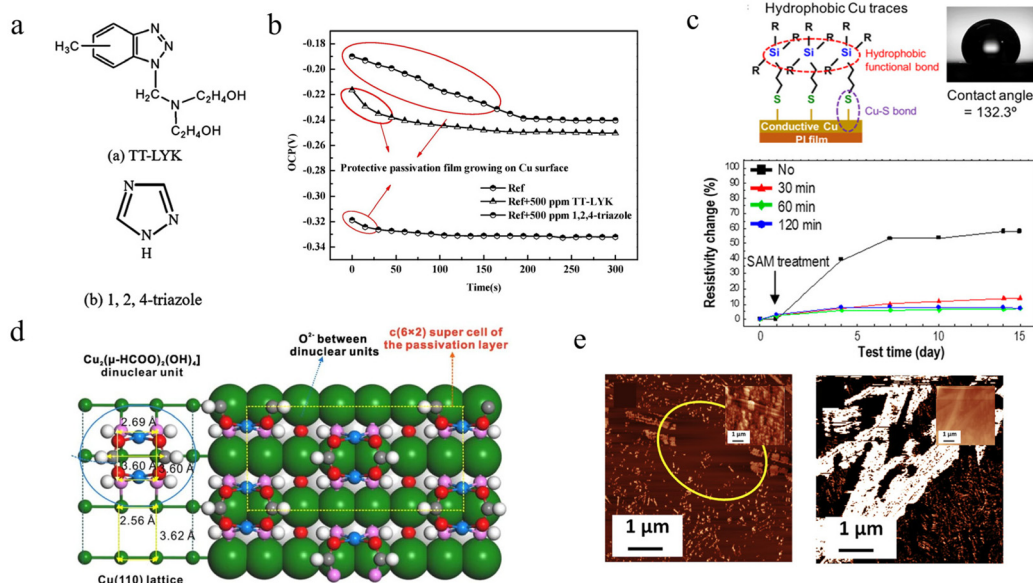
Fig. 8 Chemical protection processes. (a) Molecular formulas of TT-LYK and 1,2,4-triazole.[272] (b) Change in open circuit potential value for 1,2,4-triazole, TT-LYK, and H_2O_2.[272] Reproduced with permission from ref. 272. Copyright 2020 Elsevier. (c) Schematic of MPTS-passivated copper to improve hydrophobic contact angle and long-term stability.[191] Reproduced with permission from ref. 191. Copyright 2018 American Chemical Society. (d) Structure models of the paddle-wheel dinuclear Cu(II) formate complex and the Cu (110) surface.[274] Reproduced with permission from ref. 274. Copyright 2020 Springer. (e) Current mapping image for (left) after aging in the oven and (right) after retreatment with acetic acid.[167] Reproduced with permission from ref. 167. Copyright 2020 Elsevier.

Ni),[60,66–69,96,119,278] graphene,[217] various metal precursors (nickel formate, nickel acetylacetonate),[57,127] *etc.* The preparation options include galvanic displacement,[98,119] chemical deposition,[278] electrodeposition,[61] atomic layer deposition,[276] and thermal deposition.[63,277] In order to meet the need for higher electrical conductivity, metal shell layers are the best choice. Precious metals with oxidation resistance and high electrical conductivity such as Ag and Au are widely used in the preparation of copper core–shell structures. Based on the difference in the standard reduction potentials of silver (E_0 = 0.779 V) and copper (E_0 = 0.46 V), Lee *et al.* prepared copper–silver core–shell nanoparticles in a solution of $AgNO_3$ by galvanic displacement at 80 °C for 2 h.[119] HRTEM analysis revealed that copper element dominated the center of the nanoparticles, and the edges were dominated by silver element, as shown in Fig. 9a. Huang *et al.* found that the introduction of some smaller sized copper nanoparticles around the large copper nanoparticles could significantly shorten the time of galvanic displacement (~20 s).[98] The small-sized copper nanoparticles were used for catalytic replacement of Ag ions, while the large-sized copper nanoparticles provided nucleation sites for the growth of AgNPs.

Although galvanic displacement is the simplest method without additional reducing agents and additives, the reaction consumes copper particles, resulting in surface defects, which is not suitable for preparing CuNWs with core–shell structures. This will reduce electrical conductivity, because the reduction in diameter significantly affects the electron transport, especially when the linewidth is close to the mean free range of the elec-

trons. Stewart *et al.* found that the core–shell copper nanowires with good structure can be obtained by using chemical deposition.[278] The addition of ascorbic acid in alkaline solution inhibits the oxides and promotes the reduction of silver ions on the surface of CuNWs, leading to Cu@Ag nanowires that were stable at 160 °C and 85% RH for 24 hours. Zhang *et al.* formed a homogeneous alloy protective shell by co-depositing Au and Ag atoms in $KAu(CN)_2$ and $KAg(CN)_2$ solutions using CuNWs flexible transparent films as the cathode and graphite flakes as the anode,[61] as shown in Fig. 9b. The cyanide of Ag and Au can reduce the standard electrode potential difference from 0.7 V (Ag ~0.8 V, Au ~1.5 V) to 0.2 V, which achieves good co-deposition for excellent optoelectronic properties (14.2 Ω sq^{-1} at 90.1% transmission, 2000 times bending) and corrosion resistance (168 h in atmosphere, 200 s in H_2O_2 solution, 1800 s in sulfuric acid solution to maintain integrity). However, it is noted that the CuNWs must be immersed in the solution after the current is applied, otherwise the galvanic displacement will occur first.

The preparation of a self-assembled core–shell structure by co-reduction of various metal precursors can improve the storage and printing stability of ink. Li *et al.* reported that a simple mixture of Cu formate and Ni formate composite inks can spontaneously form Cu@Ni core–shell nanostructures after thermal annealing at 170 °C for 15 min.[127] Different decomposition temperatures of copper formate (starting at 110 °C) and nickel formate (starting at 185 °C) were found to be critical for the generation of core–shell structures by thermogravimetry-differential thermal analysis coupled with mass spectrometry (TG-DTA-MS). Moreover, the catalytic effect of
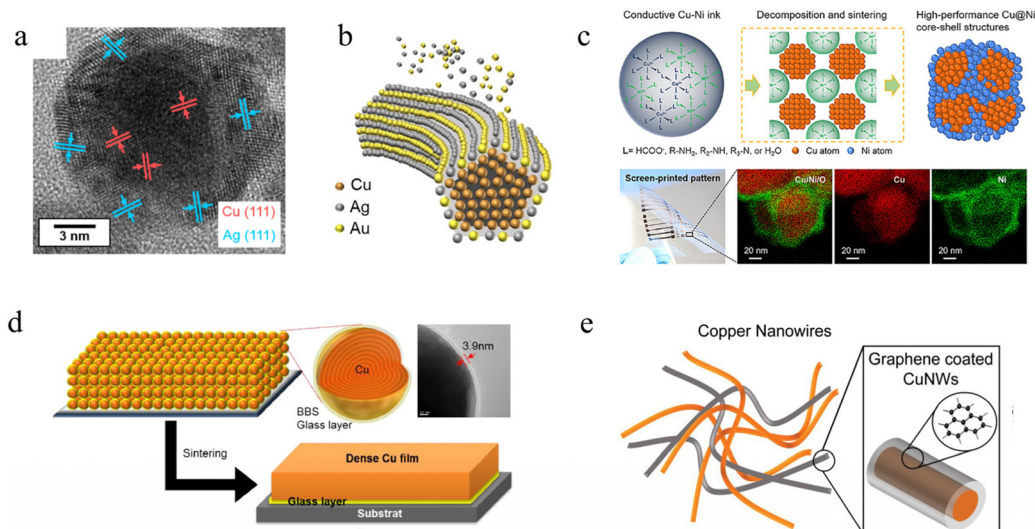
Fig. 9 The core–shell structure. (a) HRTEM image of a Cu@Ag nanoparticle.[119] (b) Schematic illustration of CuNW@alloy core–shell structure.[61] Reproduced with permission from ref. 61. Copyright 2020 Elsevier. (c) Flow chart of fabrication Cu@Ni nanoparticles by co-reduction and EDS element analysis.[127] Reproduced with permission from ref. 127. Copyright 2022 American Chemical Society. (d) Schematic image of Cu@BBS nanoparticles and the sintering for dense Cu film.[277] Reproduced with permission from ref. 277. Copyright 2021 Elsevier. (e) Schematic illustration of Cu@graphene by thermal decomposition of dopamine.[217] Reproduced with permission from ref. 217. Copyright 2021 American Chemical Society.

copper reduced the overall decomposition temperature (~170 °C). Depending on the Ni content, the printed patterns have a high electrical conductivity of 19–67 μΩ cm and high oxidation resistance at 180 °C ambient conditions.

Cu-shell structures can also be prepared by using inorganic compounds or carbon materials. Tigan *et al.* used atomic layer deposition (ALD) to prepare CuNWs@Al_2O_3/ZnO.[276] Compared with conventional bare CuNWs transparent film heaters (~100 °C), the shell layer protection allowed the upper heating limits to be raised to 273 °C and 204 °C with uniform heating. Xiao *et al.* used microwave-induced metal dissolution to synthesize CuNWs@ZnS, and the visible light response due to the narrowing of the band gap enabled the H_2 evolution rate to reach 10 722 μmol h^{-1} g and the quantum efficiency to reach 69% under 420 nm LED light irradiation.[63] Jung *et al.* used ultrasonic spray pyrolysis to achieve large-scale preparation of Cu@barium borosilicate (BBS) glass particles.[277] The melting point difference between metallic copper and BBS glass formed a core–shell structure with a shell layer only 3.9 nm thick. The sintering process with BBS glass as binder and accelerator achieved good adhesion of copper to the substrate and high-density patterning with a film resistivity of 2.01 μΩ cm (very close to the resistivity of pure copper), which only increased to 2.26 μΩ cm after one month exposure to air. The excellent electrical and thermal conductivity of graphene mean that it can also be used as a shell layer material. Dopamine stirred in copper ink can decompose at high temperatures to produce graphene shell layers *in situ*, but annealing temperatures above 800 °C are only applicable to highly temperature-resistant substrates, such as ceramics.[150,217]

4.2.2. The coating structures. Although the core–shell structure has achieved excellent results for comprehensive pro-

tection of individual Cu particles from oxidation, the nano-scale processing and manufacturing bring problems such as long cycle time, high cost, and poor compatibility. The coating structure directly adds a large protective layer to the printed copper film to prevent contact between oxygen, water, and other substances with copper. With the characteristics of fast, low cost, and compatibility with the R2R process, it is an alternative for future industrial manufacturing of high-oxidation-resistance copper inks. The coating structure here is not limited to the deposition of a protective layer on the surface of the printed copper film, but extends to the hybridization of the internal structure of the copper film to improve the durability of the necked joints. The materials used for the coating are generally organic polymer substances,[77,166,169] graphene,[113,170] metals,[120,133] oxides,[171] *etc.* The strong interaction of the organic polymer with the copper surface and its excellent mechanical properties can effectively isolate the copper from the external environment without peeling off, and the operability of the organics can give the coatings special properties, such as corrosion resistance. Mock *et al.* prepared high-performance CuNWs transparent conductive films (7.6 Ω sq^{-1} at 77% transmittance) in oleylamine solution and used PDMS and PMMA coatings with electron beam evaporation of SiO_2 and Al_2O_3 to protect CuNWs from oxidation.[166] It was found that the stability of the PDMS-coated CuNWs films decreased, which was attributed to the high permeability of PDMS to air and the chemical reaction with CuNWs. On the contrary, as coatings, PMMA, SiO_2 and Al_2O_3 can effectively improve the service life of CuNWs. Modifying the polymer surface with a low permeability oxide layer retains the excellent mechanical properties of the polymer and also solves the oxidation problem caused by high water permeability.

Considering the oxidation problem of water molecules from microcracks and pinhole leakage of PI, Hong et al. spin-coated PI resin on prepared copper nanowire films and deposited a 100 nm thick SiO_x layer on the PI layer as a sealing layer,[279] as shown in Fig. 10a. The comparison revealed that CuNWs with the SiO_x sealing layer showed almost no change in heating resistance at high temperature over 320 °C and also had electrical properties comparable to those of AgNWs after 7 days under a humid environment. However, this method introduces an additional process of depositing the coating. Organic coatings can be electropolymerized on copper surfaces by voltammetric cycling in acidic solutions. Ma et al. electropolymerized PANi, PNEA, and molybdate-doped PANi-Mo and PNEA-Mo coatings on copper surfaces in oxalic acid solutions.[280] The XPS and molecular dynamics analysis revealed that the introduction of the ethyl group in the organic polymer backbone reduces the physical defects of the coating, and the molybdate doping further reduces the porosity of the coating and repel the cations in the solution to maintain the charge balance inside the coating, as shown in Fig. 10b.

The excellent electrical conductivity, light transmission, and high sealing properties of graphene make it ideal as a coating material. Lu et al. used the plasma enhanced chemical deposition (PECVD) process to deposit graphene on copper ink to achieve copper ink reduction, sintering, and passivation in one step.[113] Conductive copper patterns with a resistivity of 0.03762 mΩ cm were produced at an optimal ratio of H_2/CH_4 = 8. This rapid preparation using the integrated coating and sintering process is favorable for large-scale copper ink applications. However, problems such as steps and defects at the polycrystalline copper interface affect the graphene adhesion stability, and defects such as voids and folds after polycrystalline graphene adhesion do not effectively prevent the contact of corrosive elements (O_2, H_2O) with copper. Wang et al. prepared transparent conductive films with a UV-curable resin–CuNWs–monocrystalline graphene structure.[170] CVD was used to deposit a single monocrystalline graphene layer on copper (111) foil. The perfect interface of Cu (111) allows the single-crystal graphene to be seamlessly stitched together to form a continuous network, giving the CuNWs transparent conducting network excellent electrical properties (19 Ω sq^{-1}, 84.3% transmittance) and oxidation resistance ($\Delta R/R_0$ < 0.2 after 180 days under ambient conditions). However, controlling the growth of this graphene and additional wet etching of the copper foil increases the cost of using this process, which is still a challenge in applying to industrial production.

In addition, metal fillers as coating materials can also effectively improve the durability of copper inks, which is related to the copper particle sintering process.[120,121,123] Sintering drives the movement of the outer atoms of copper and the nearby atoms to combine to form a neck connection. Owing to the smaller diameter and increased contact area, the Cu neck connection is usually fragile. The additional metal filler acts as a bridging agent for the independent copper source during the sintering process, reducing the disadvantages of easy oxidation and poor mechanical toughness caused by the copper neck connection. The commonly used metal fillers are Ni, Sn, and Ag due to their lower melting points and better stability than Cu. Chen et al. developed a Cu/Sn hybrid ink. The low melting point of Sn allowed for a 21% reduction in the energy required for IPL sintering while achieving good connectivity around the Cu nanoparticles (14 Ω sq^{-1}).[131] Cu/Sn inks achieved better adhesion after sintering compared to pure Cu inks and were almost defect-free when prepared at ultrafine line widths (3.5 μm). Chung et al. used electro-explosion to prepare Cu/Ag
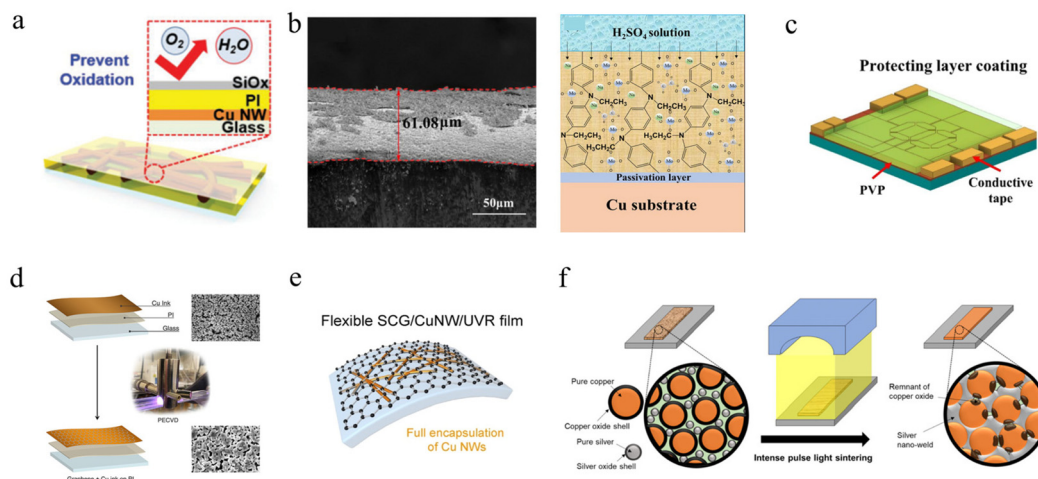

Fig. 10 Coating structure. (a) Schematic illustration of CuNWs/PI/SiO_x composite film.[279] Reproduced with permission from ref. 279. Copyright 2019 John Wiley and Sons. (b) Cross-section SEM of PNEA-Mo coating and schematic of the anticorrosion mechanism of PNEA-Mo coating in H_2SO_4 solution.[280] Reproduced with permission from ref. 280. Copyright 2020 Elsevier. (c) Schematic diagram of coating a PVP layer onto a Cu electrode.[169] Reproduced with permission from ref. 169. Copyright 2020 Elsevier. (d) Schematic of coating graphene on Cu film by PECVD.[113] Reproduced with permission from ref. 113. Copyright 2021 American Chemical Society. (e) Schematic of the flexible SCG/CuNWs/UVR composite film.[170] Reproduced with permission from ref. 170. Copyright 2020 Elsevier. (f) Schematic of the welding process by AgNPs via IPL.[121] Reproduced with permission from ref. 121. Copyright 2021 American Chemical Society.

hybrid nanoparticles (4.06 μΩ cm) on PI substrates under optimized voltage conditions and flash sintering light energy, and the conductive patterns were able to exist stably for more than 15 h when heated at 100 °C.[133]

5. Applications

The remarkable electrical properties of copper-based inks have motivated their applications for electronic components, such as flexible transparent heaters (FTHs),[96,276,279] transparent conductive electrodes (TCEs),[158,281] sensors,[217,266] thin-film transistors,[93,117] photovoltaic devices[147,170] and antennas.[65,125] Here, we will briefly summarize the recent progress in the development of copper-based functional electronics.

5.1. Transparent conductive electrodes (TCEs) and flexible transparent heaters (FTHs)

Conventionally used transparent electrodes of ITO have disadvantages such as high price, rigidity, and preparation requirements. CuNWs have become the most promising alternative to ITO in achieving high conductivity and high transmission owing to the high aspect ratio.[158,160,276] Although CuNWs are non-transparent, the high aspect ratio allows them to achieve lateral conductivity with a low duty cycle. The quality of the sample can be measured by the sheet resistance (R_s) and the transmittance (T_g) under 550 nm wavelength. The figure of merit (FoM) is defined as:[282]

$$\text{FoM} = \frac{188.5}{R_s\left(\dfrac{1}{\sqrt{T_g}} - 1\right)}$$

The FoM values calculated for some TCEs are compiled in Table 2. Tran *et al.* used a nanosecond pulsed laser to sinter CuNWs for the selective preparation of high-performance TCEs.[169] The laser energy density and scanning speed were optimized by simulation to eliminate thermal damage to the flexible substrate, and the obtained CuNWs TCEs had a sheet resistance of 60 Ω sq^{-1} and a transmittance of 93.6% at 550 nm. Acetic acid immersion removes impurities such as copper oxide and PVP, resulting in a 5% increase in the resistance of the transparent electrode at 1500 cycles with a 10 mm bend radius. Zhong *et al.* prepared large-scale CuNWs TCE (22.1 Ω sq^{-1}, 85.6% transmittance), IPL irradiation of CuNWs self-embedded in plastic substrates provided excellent mechanical toughness (10 000 cycles of bending durability and over 120 hours of resistance stability under ambient conditions) so that the LEDs can stably illuminate even under bending and pasting,[160] as shown in Fig. 11a. Alternatively, TCEs can be prepared by artificially controlling the duty cycle of copper traces to achieve a mesh structure.[131] Kwon *et al.* prepared a conductive copper network with a line width of 20 μm and a blank width greater than 200 μm using selective laser sintering of CuNPs ink coated on PEN.[283] The conductivity of the copper pattern was 1.67×10^{-4} Ω m, and at a bending radius of 2.25 mm it could be continuously cycled 1000 times, as shown in Fig. 11b.

Due to the resistance Joule effect $Q = V^2 \times t/R$, transparent heaters can be used for defrosting and de-icing displays and composite glass for LCDs, billboards, and vehicles.[96,276] Hong *et al.* prepared CuNWs transparent conductive film with water and oxygen barrier (relative resistance change less than 0.3 times after 7 weeks of immersion in water).[279] A uniform heating case of 132.7 °C can be obtained at 10 V. Even if the
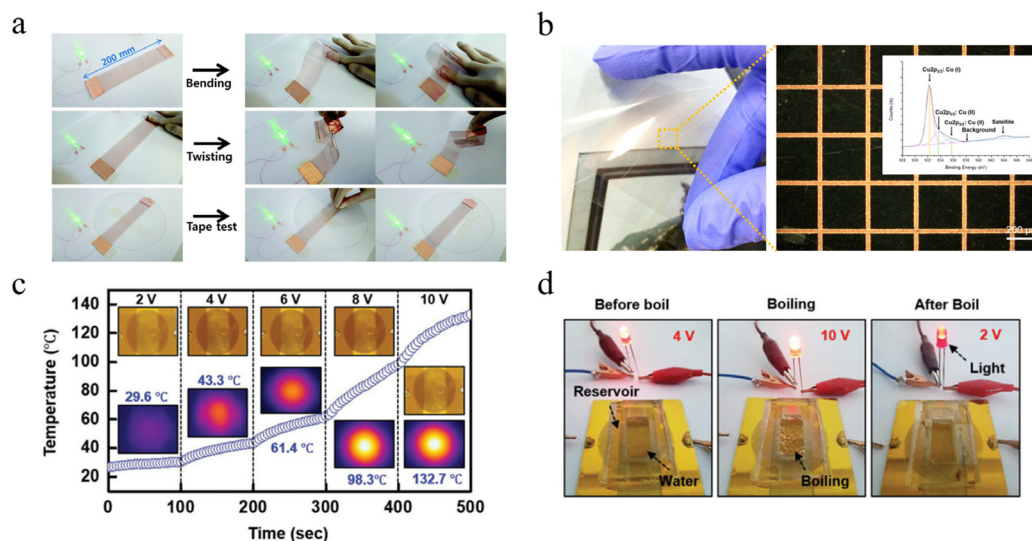

Fig. 11 (a) Photographs of the LED circuit with TCE.[160] Reproduced with permission from ref. 160. Copyright 2016 Royal Society of Chemistry. (b) Optical image of Cu grid transparent conductor.[283] Reproduced with permission from ref. 283. Copyright 2016 American Chemical Society. (c) Time-dependent temperature curves of FTH by applying voltage.[279] (d) Photographs of water boiling before and after being heated by FTH.[279] Reproduced with permission from ref. 279. Copyright 2019 John Wiley and Sons.

PDMS mill is filled with water above, it can be heated to boil water without affecting the light intensity change of the series LED lamps, as shown in Fig. 11c and d. Zhong *et al.* prepared FTHs heaters using a roll-to-roll process combined with IPL irradiation; the temperature distribution was uniform under the applied voltage, and the temperature rise with the voltage rise would reach saturation within 70 s.[212] Bobinger *et al.* prepared FTHs (R_s = 10.3 Ω sq^{-1}, T = 83.4%) by inkjet using copper chloride as a precursor for the preparation of CuNWs.[164] The FTHs were able to be heated uniformly and the resistance remained well linear with temperature. Subsequently, they prepared a heating film using a similar copper nanowire system and applied it to a thermoacoustic loudspeaker for the first time (the response was in good agreement with the simulation fit).[165] Although the copper FTHs can obtain a good heating effect and fast response time, copper is easily oxidized at high temperatures, leading to a severe decrease in its electrical conductivity.

5.2. Sensors

Copper ink applied by printing techniques can be directly used as a flexible sensor to detect physiological and physical signals, which can be used for the expensive metal sensing components in commercial applications.[64,150,155,168,191] The excellent mechanical toughness of CuNWs is widely used in the field of strain sensors. Zhang *et al.* prepared CuNWs@IOnGel composite films with porous structure using PS microspheres.[266] The porous structure created by the PS microspheres within the gel improves the compressibility of the film and exhibits extremely high sensitivity as a pressure sensor (S = 39.7 kPa^{-1} in the range of 0.7–1000 Pa). The embedded structure of nanowires and gels provides the sensor with good mechanical stability (3000 finger bending cycles). They demonstrated the composite film as a sensor to monitor human physiological signals, effectively identifying three TCM static pulse waves (Chen, Zhong, and Fu), as shown in Fig. 12a. Khuje *et al.* prepared CuNWs pressure sensors on piezoelectric ceramics.[217] The array of sensors was attached to the surface of human skin to monitor small pulse signals. The sensing mechanism can be explained by the fact that the longitudinal pressure forces the presence of more CuNWs contact points at the upper and lower interfaces, providing more channels for electron transport and leading to a decrease in film resistance, as shown in Fig. 12b and c. Kwon *et al.* inkjet-printed copper inks with high adhesion on PI substrates.[191] It has high oxidation resistance (stable under ambient conditions for more than 15 days) while maintaining ultra-high mechanical durability (100 000 bending cycles). In the absence of conductive gel, the copper electrodes are capable of stable measurement of ECG, EMG and EOG signals. Wearable electronic devices also need to work stably for the long-term. Zhang *et al.* showed highly conductive (0.808 Ω sq^{-1}) and flexible (1000 bending cycles) composite films obtained using reduced graphene oxide (RGO) and CuNWs.[284] By depositing on polyester cloth, the thin and light flexible circuits can be used for LED lighting for long periods of time (>30 days under ambient conditions).

The higher sensitivity and lower oxidation potential of copper are also widely used in electrophysiological applications. Redondo *et al.* demonstrated for the first time the application of 3D-printed pure copper electrodes prepared
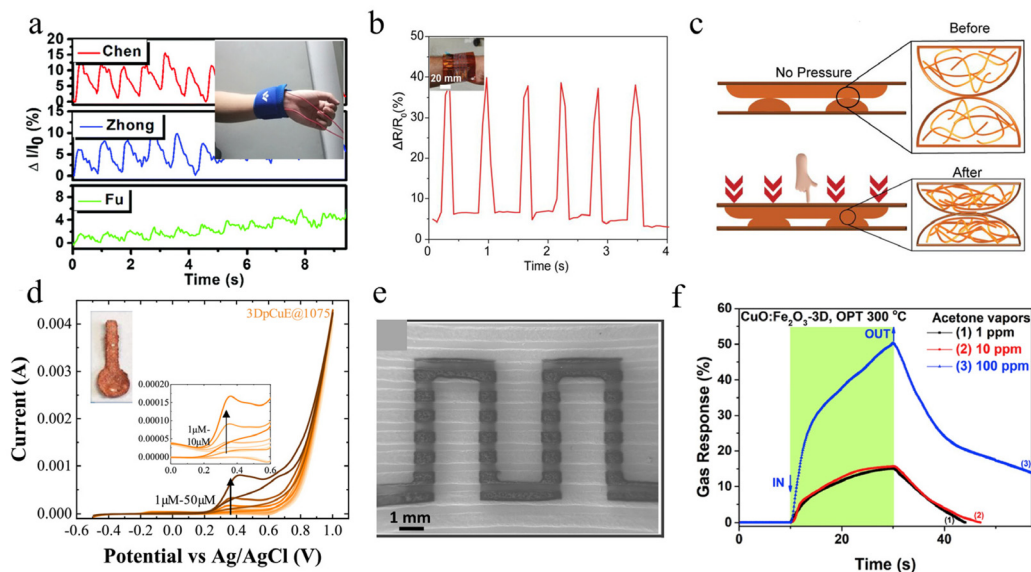

Fig. 12 (a) Three different test pressures by TCM are defined. Inset: Photograph of tester's pulse test.[266] Reproduced with permission from ref. 266. Copyright 2020 Royal Society of Chemistry. (b) Plot depicting the sensor performance for characterizing the arterial pulse. Inset: Photograph of tester's pulse test.[217] Reproduced with permission from ref. 217. Copyright 2021 American Chemical Society. (c) The sensing mechanism of the resistive pressure sensor.[217] Reproduced with permission from ref. 217. Copyright 2021 American Chemical Society. (d) Cyclic voltammograms of different concentrations of glucose. Inset: Photograph of the sensor.[264] Reproduced with permission from ref. 264. Copyright 2020 Elsevier. (e) SEM of acetone sensor.[211] (f) Dynamic response at operating temperature of 300 °C to 1, 10 and 100 ppm of acetone vapor.[211] Reproduced with permission from ref. 211. Copyright 2020 Elsevier.

using fused filament fabrication (FFF) for non-enzymatic sensing of glucose.[264] By optimizing the sintering temperature to obtain the highest purity copper film, the sensor exhibited a wider linear range (1–50 μM), lower monitoring limit (0.06 μM), and higher sensitivity (0.03 μM^{-1} cm^{-2}) compared to other copper-based systems, as shown in Fig. 12d. Siebert *et al.* mixed micron-sized copper and iron powders through 3D printing to form a continuous pattern, thermally annealed in the air to form a heterojunction structure of metal oxides.[211] Based on the physicochemical changes occurring at different temperatures, the sensor has good selectivity for acetone vapor at an operating temperature of 300 °C with a gas response of 50% at 100 ppm vapor concentration and a minimum power consumption of 0.26 μw, as shown in Fig. 12e and f. The excellent performance is attributed to the metal oxide pinpoint contact porous bridging structure.

5.3. Optoelectronic devices

In order to prepare flexible optoelectronic devices, flexible conductive electrodes must first be prepared. Copper ink can be printed on a variety of flexible substrates (PET, PEN, PES) to give the traditional rigid electrodes bendable and foldable characteristics, and its low cost and high conductivity mean it is the main material to replace precious metal (Ag, Au) electrodes,[28,29] as shown in Fig. 13. Yang *et al.* developed a bottom electrode for a flexible perovskite solar cell (PSC) by depositing a protective layer of ZnO with Al doping (AZO) on the CuNWs transparent conducting electrode using atomic layer deposition (ALD).[171] While retaining excellent electrical properties (34.05 Ω sq^{-1}, 87.77% transmittance at 550 nm), the protective layer of AZO also effectively prevents the diffusion of iodine ions from perovskite into the CuNWs electrode to induce the decomposition of NWs (almost no change in resistance after 7 days of exposure to the perovskite layer). The power conversion efficiency (PCE) of the PSCs prepared based on this composite electrode was 14.18% and the filling factor (FF) was 70.77% by improving the energy band arrangement in the interfacial layer. Moreover, the PCE changed non-significantly after 600 cycles at 12.5 mm bending radius. Im *et al.* first demonstrated flexible OLED devices using CuNW transparent conductive electrodes.[147] High-performance fiber-reinforced transparent plastic conductive films (R_s = 25 Ω sq^{-1}, transmission = 82%) were prepared by encapsulating CuNWs with UV light-curable resin. Even after 10 000 cycles at a bending radius of 5 mm and 14 days of aging test at 80 °C, there was no significant change in resistance. The prepared windmill-shaped OLEDs achieved a maximum luminance of about 10^4 cd m^{-2} at a driving voltage of 9 V with a current density much higher than 10^2 mA cm^{-2}, and can stably emit green light under bending. Wang *et al.* prepared flexible OLEDs using a single layer of monocrystalline graphene and UV-curable resin to protect CuNWs for improved durability as an anode output.[170] Compact coverage of CuNWs with a single graphene layer results in electrodes with good mechanical durability (>1000 cycles) and long-term stability (<0.2 times change in resistance after 100 days under ambient conditions).

The composite film has a higher work function (4.87 eV) compared to the ITO (4.7 eV) anode, which increased the hole
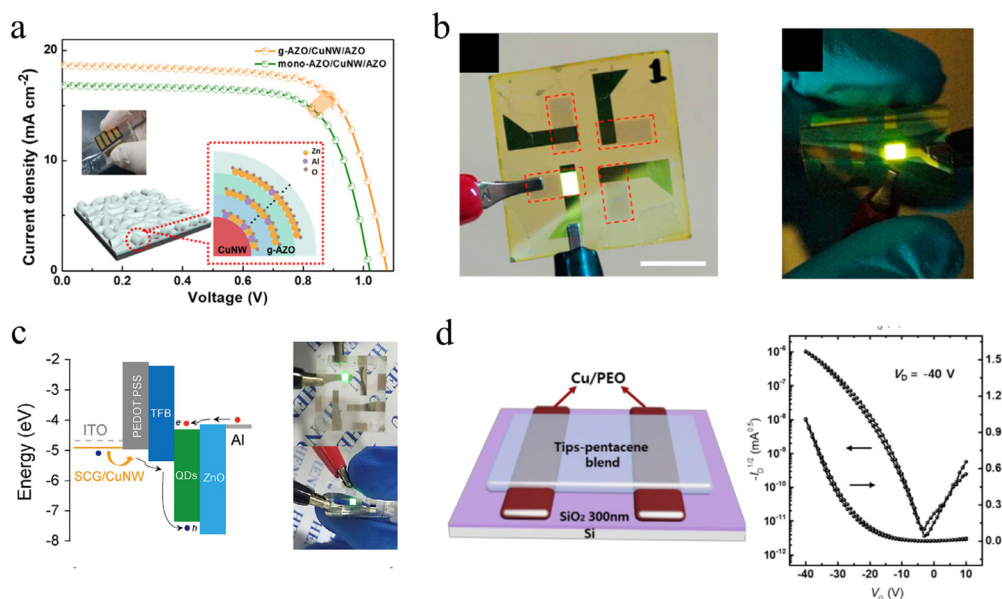

Fig. 13 (a) The *J*–*V* curves of flexible PSCs based on different electrodes. Inset: Photograph of flexible PSC and schematic diagram of doping Al.[171] Reproduced with permission from ref. 171. Copyright 2020 American Chemical Society. (b) Photograph of OLED device operating in (left) flat and (right) flexed states.[147] Reproduced with permission from ref. 147. Copyright 2014 American Chemical Society. (c) Energy band diagram of the OLED device (left) and photograph of the OLED operating in different states (right).[170] Reproduced with permission from ref. 170. Copyright 2020 Elsevier. (d) Schematic image of the OFETS (left) and transfer characteristics of OFETs (right).[285] Reproduced with permission from ref. 285. Copyright 2020 Elsevier.

injection rate and the luminance to 8760 cd m^{-2} at a current density of 4.25 cd A^{-1}. This is much higher than the OLED with flexible ITO (1.2 cd A^{-1} at 5883 cd m^{-2}).

Similarly, CuNP inks play an important role in opto-electronic devices. In contrast to the CuNWs thin-film approach, a controlled Cu grid trace is used to replace ITO electrodes. This has the great advantage of reducing the cost of production, knowing that the synthesis of CuNWs is much more complex than CuNPs. Georgiou *et al.* prepared the first OPVs using CuNPs ink as a substrate electrode by using inkjet-printing.[286] The best PCE value of 3.35% was obtained when the number of Cu grids was six (17% c overage, J_{sc} = 11.39 mA cm^{-2}, FF = 50.72%). However, this Cu electrode oxidizes rapidly at 160 °C in an air environment, leading to device failure, and the exposed Cu electrode will cause large leakage currents owing to the line height and surface roughness. One year later, the same group prepared the first ITO-free OLED based on a CuNPs/PEDOT:PSS hybrid substrate electrode with an improved process.[287] Instead of depositing copper ink directly on the substrate, they chose to pre-deposit it on the glass substrate and then transfer it to the substrate by the reverse nanoimprinting transfer method to form embedded Cu grids. The biggest advantage of this approach is that it results in a flatter surface for the electrodes, reducing leakage current and thus increasing efficiency, resulting in a maximum CE of 3.6 cd A^{-1}. In the same way, Kamijo *et al.* demonstrated high-resolution OLEDs with CuNPs grids as the bottom electrodes.[288] The OLED luminescence intensity in the case of CuNPs ink traces with small pitch (<5 μm) and narrow line widths (0.5 μm) was close to that of the ITO reference. Similar to the previous work, a thickly doped hole injection layer is used to reduce the roughness of the Cu gate electrode and avoid short circuits.

5.4. Thin-film transistors

Thin-film transistors are the basic components of smart-phones and other electronic displays.[289,290] Although there have been many studies on the trench layer, there are disadvantages of complicated processes (magnetron sputtering, vapor deposition) and expensive materials (gold, silver) for the deposition of the source–drain connecting the trench.[291,292] Copper can solve the high cost problem owing to its high resistivity and low price, and the transistors obtained by printing can also exhibit properties such as flexibility and stretchability. Can *et al.* used EHD to print a copper source–drain on ZTO under vacuum sintering (380 °C) for transistors.[117] The average effective mobility in the saturation region was 0.50 cm^2 V^{-1} s^{-1} with an on-to-off current ratio of 5.5 × 10^5. Li *et al.* investigated the effect of different ratios of poly(ethylene oxide) on the viscosity of copper nanoplate ink and prepared organic field-effect transistors on SiO$_2$ substrates in combination with IPL sintering.[285] The average field-effect mobility was 0.253 cm^2 V^{-1} and the on/off current ratio was 10^6.

5.5. Flexible circuits

Flexibility is the goal of future electronic devices. Lightweight, easy to produce, and reliable complex integrated systems require highly conductive, low-cost interconnection paths.[293,294] Copper ink is the most promising material for preparing flexible circuits, which can be achieved by printing on flexible substrates (PET, PEN, PES). Zareei *et al.* prepared flexible circuit-lit LEDs by screen printing copper–silver hybrid inks on PET.[121] The lowest porosity of 1.2% and square resistance of 0.072 Ω sq^{-1} were obtained with an AgNPs content of 16 wt% and IPL sintering photon energy density of 10.6 J cm^{-2}. This gave the best adhesion to PET substrate without
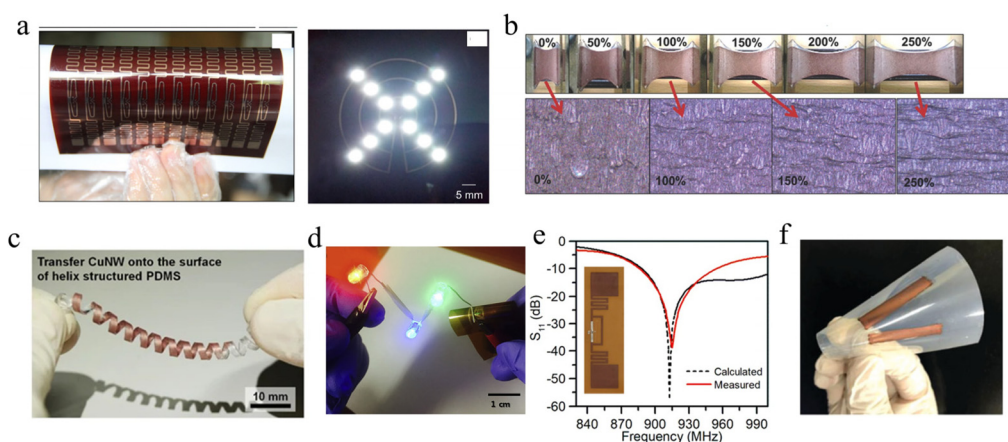

Fig. 14 (a) Photograph of flexible Cu pattern on PI substrate (left) and operation of LED chips connected to conductive Cu patterns.[189] Reproduced with permission from ref. 189. Copyright 2017 Elsevier. (b) Stretchability test of the CuNWs conductor.[252] Reproduced with permission from ref. 252. Copyright 2014 John Wiley and Sons. (c) Photograph of the helical-structured CuNWs electrodes.[163] Reproduced with permission from ref. 163. Copyright 2014 Springer. (d) The printed Cu ink on the PI substrate lights the LED under bending conditions.[95] Reproduced with permission from ref. 95. Copyright 2018 Elsevier. (e) Calculated and measured S11 results of the fabricated UHF dipole tag antennas. Inset: Photograph of the UHF dipole RFID tag.[112] Reproduced with permission from ref. 112. Copyright 2022 Springer. (f) Photograph of Cu V-shaped dipole antenna.[125] Reproduced with permission from ref. 125. Copyright 2019 John Wiley and Sons.

peeling even after pasting by tape, and maintained high conductivity for 7 days even under harsh conditions (70 °C, 100% RH). Chen *et al.* prepared copper patterns (14.3 μm thickness and 5.68 μΩ cm) on PI substrates by inkjet printing with a two-step chemical plating process.[189] The Cu pattern printed on the PI substrate has smooth edges, exhibits a distinct metallic luster, and can be bent many times. Even after one year of operation, the LEDs continue to light up, as shown in Fig. 14a. Son *et al.* prepared flexible circuits (2.1×10^{-7} Ω m and 100 μm line width) using copper nanoparticle inks protected by 1-octanethiol coating.[95] The circuit is stable under environmental conditions for 2 months and can withstand 1000 cycles of bending tests. Good electrical conductivity was achieved by stable lighting of the LEDs even after bending, as shown in Fig. 14d. Stretchable copper electrodes have been reported. Han *et al.* prepared highly flexible conductors using laser-welded CuNWs on Eco-Flex films under ambient conditions.[252] The conductive films obtained by this method were able to maintain a stable resistance at 250% stretching and for 20 000 bending cycles compared to conventional thermal annealing, which causes warping and rupture of the films, as shown in Fig. 14b. Won *et al.* prepared spiral PDMS mills by casting and then transferred CuNWs to the mills to obtain stretchable conductors with a special structure,[163] as shown in Fig. 14c. The relative resistance of this conductive spring changed by only 3.9% at 700% stretching.

5.6. Antenna RF tags

Copper inks are also widely used in flexible antennas and radio frequency identification (RFID) tags.[65,66,114,127,238] Hong *et al.* used formate and thiol-passivated copper paste (with a conductivity of 13 400 S cm^{-1}) to fabricate an ultra-high-frequency (UHF) RFID tag by screen printing. The resistance of the passivated copper electrode was stable at 60 °C for more than 500 hours and the dipole antenna has a maximum gain of −2 dB, a reflection coefficient (S_{11}) of −38 dB, and good applicability on PI, paper, and fabric substrates (read ranges of 12.8, 11.3, and 7.7 m, respectively);[112] the S_{11} of RFID is shown in Fig. 14e. Zhang *et al.* used a composite ink system comprising copper nanowires and copper precursor sintered at low temperature (140 °C) to obtain conductive patterns with resistivity of 14.9 μΩ cm. V-Shaped dipole antennas (length = 30 mm, width = 5 mm, and angle of 30°) were printed on PET, and the antenna return loss was tested at 2.3 GHz at about 32 dB.[125]

6. Summary and outlook

Copper inks are widely used in the field of flexible printing, with the advantages of low-cost and good electrical conductivity, and are the best substitute for precious metal inks, such as silver. This paper reviewed the research progress of copper-based inks in flexible electronics in recent years, discussed the process improvement of copper ink preparation, printing, and sintering, summarized the methods to improve the conduc-

tivity and durability of copper patterns after film formation, and introduced the emerging applications of copper inks in flexible electronic devices, such as transparent electrodes, sensing, optoelectronic devices, and antennas. Although encouraging progress has been made in the development of copper inks, there are still two major problems in the application of next-generation electronic devices: the feasibility of printing patterns and long-term stability.

It is still difficult to achieve effective sintering of copper inks on some thermal substrates (PET, PEN), and regulating the parameters of sintering for different ink systems increases the complexity of the preparation process. Copper precursor inks may be a feasible solution to achieve efficient printing and low-temperature sintering. The ionic form avoids blocking the mesh or nozzle during printing and oxidation during storage, and selecting precursors with low decomposition temperature can avoid damage to the flexible substrate during the sintering process. Photonic sintering is an effective method for large-area preparation owing to its advantages of speed and low cost, but high-energy pulsed light may cause local excess heat, which needs further optimization during operation.

The reliability of copper inks in applications is also a major issue of current research. Additives and the copper content in the ink can affect the porosity, surface defects, and step flatness of the film after sintering. Passivation is a simple method that can be operated on a large scale. The development of formic acid roots promises high oxidation resistance without compromising conductivity. However, the formation of dense passivation layers requires the provision of epitaxial copper boundaries with a tight, flat structure, which prevents passivation from improving in efficiency. The rapidity and compatibility of coating protection mean that it could be a future solution to achieve stable copper use, but the preparation process needs to be optimized to improve the degree of wrapping at the interface between the coating and copper.

In addition, adhesion and resolution are also issues that need to be overcome. The degree of adhesion of the copper ink to the flexible substrate determines whether it can work stably in bending and folding situations. This can be improved by adding cellulose to the ink or pretreating the flexible substrate to improve the bonding with the copper molecules. High resolution is a requirement for the miniaturization of printed electronic devices. EHD jet printing and laser sintering are good choices, but the complexity and high cost of the equipment do not match the advantages of copper, causing it to be difficult to achieve in industrial production.

In general, significant progress has been made in the development of copper-based inks. For printability problems, many new methods have been proposed regarding raw materials and additives to obtain uniformly dispersed and easily stored inks. For conductivity problems, methods such as passivation layers and coatings have been proposed to reduce or avoid the generation of oxides. We investigated the development of various conductive inks in the market and predict that the share of copper inks will gradually equal that of the mature and stable

silver inks in the next 10 years, with a 30% share of the total.[295] The future development of wearable electronic devices will require not only flexibility but also stretchability. Although CuNWs have made progress in the research of stretchable composite elastomers, Cu nanosheets/micron sheets with lower cost are still far from silver composite elastomers in achieving high stretchability. We hope that future research will propose new solutions for the preparation and printing methods of copper-based inks to achieve a printing system with good stability, cost-effectively with a simple process and low waste production, which can promote the development of copper-based ink in the field of flexible printed and wearable electronics.

Conflicts of interest

There are no conflicts to declare.

Acknowledgements

References

1 N. Karim, S. Afroj, D. Leech and A. M. Abdelkader, *Oxide Electron.*, 2021, 21–49.

2 J. Perelaer, P. J. Smith, D. Mager, D. Soltman, S. K. Volkman, V. Subramanian, J. G. Korvink and U. S. Schubert, *J. Mater. Chem.*, 2010, **20**, 8446–8453.

3 S. Afroj, L. Britnell, T. Hasan, D. V. Andreeva, K. S. Novoselov and N. Karim, *Adv. Funct. Mater.*, 2021, **31**, 2107407.

4 S. Xu, Z. Yan, K.-I. Jang, W. Huang, H. Fu, J. Kim, Z. Wei, M. Flavin, J. McCracken and R. Wang, *Science*, 2015, **347**, 154–159.

5 N. Matsuhisa, M. Kaltenbrunner, T. Yokota, H. Jinno, K. Kuribara, T. Sekitani and T. Someya, *Nat. Commun.*, 2015, **6**, 1–11.

6 M. Yafia, S. Shukla and H. Najjaran, *J. Micromech. Microeng.*, 2015, **25**, 057001.

7 C. Cho and Y. Ryuh, *Sens. Actuators, A*, 2016, **237**, 72–80.

8 C. D. Dimitrakopoulos and P. R. L. Malenfant, *Adv. Mater.*, 2002, **14**, 99–117.

9 E. Bacher, S. Jungermann, M. Rojahn, V. Wiederhirn and O. Nuyken, *Macromol. Rapid Commun.*, 2004, **25**, 1191–1196.

10 S. Magdassi, M. Grouchko and A. Kamyshny, *Materials*, 2010, **3**, 4626–4638.

11 K. Chen, W. Gao, S. Emaminejad, D. Kiriya, H. Ota, H. Y. Y. Nyein, K. Takei and A. Javey, *Adv. Mater.*, 2016, **28**, 4397–4414.

12 W. Wu, *Nanoscale*, 2017, **9**, 7342–7372.

13 Q. Huang and Y. Zhu, *Adv. Mater. Technol.*, 2019, **4**, 1800546.

14 L. Nayak, S. Mohanty, S. K. Nayak and A. Ramadoss, *J. Mater. Chem. C*, 2019, **7**, 8771–8795.

15 N. Karim, F. Sarker, S. Afroj, M. Zhang, P. Potluri and K. S. Novoselov, *Adv. Sustainable Syst.*, 2021, **5**, 2000228.

16 J. Song and H. Zeng, *Angew. Chem., Int. Ed.*, 2015, **54**, 9760–9774.

17 M. L. R. Liman, M. T. Islam and M. M. Hossain, *Adv. Electron. Mater.*, 2021, 2100578.

18 M. R. Islam, S. Afroj, C. Beach, M. H. Islam, C. Parraman, A. Abdelkader, A. J. Casson, K. S. Novoselov and N. Karim, *iScience*, 2022, **25**, 103945.

19 T. Q. Trung and N. E. Lee, *Adv. Mater.*, 2016, **28**, 4338–4372.

20 W. Yang and C. Wang, *J. Mater. Chem. C*, 2016, **4**, 7193–7207.

21 D. Zhang, B. Chi, B. Li, Z. Gao, Y. Du, J. Guo and J. Wei, *Synth. Met.*, 2016, **217**, 79–86.

22 X. Xu, M. Luo, P. He, X. Guo and J. Yang, *Appl. Phys. A*, 2019, **125**, 1–7.

23 P. He, J. Cao, H. Ding, C. Liu, J. Neilson, Z. Li, I. A. Kinloch and B. Derby, *ACS Appl. Mater. Interfaces*, 2019, **11**, 32225–32234.

24 X. Xu, Y. Chen, P. He, S. Wang, K. Ling, L. Liu, P. Lei, X. Huang, H. Zhao and J. Cao, *Nano Res.*, 2021, **14**, 2875–2883.

25 X. Liang, H. Li, J. Dou, Q. Wang, W. He, C. Wang, D. Li, J. M. Lin and Y. Zhang, *Adv. Mater.*, 2020, **32**, 2000165.

26 S. Lu, J. Zheng, J. A. Cardenas, N. X. Williams, Y.-C. Lin and A. D. Franklin, *ACS Appl. Mater. Interfaces*, 2020, **12**, 43083–43089.

27 T. Zhong, N. Jin, W. Yuan, C. Zhou, W. Gu and Z. Cui, *Materials*, 2019, **12**, 3036.

28 A. Kamyshny and S. Magdassi, *Small*, 2014, **10**, 3515–3535.

29 A. Kamyshny and S. Magdassi, *Chem. Soc. Rev.*, 2019, **48**, 1712–1740.

30 Y. Wang, C. Zhu, R. Pfattner, H. Yan, L. Jin, S. Chen, F. Molina-Lopez, F. Lissel, J. Liu and N. I. Rabiah, *Sci. Adv.*, 2017, **3**, e1602076.

31 S. Savagatrup, E. Chan, S. M. Renteria-Garcia, A. D. Printz, A. V. Zaretski, T. F. O'Connor, D. Rodriquez, E. Valle and D. J. Lipomi, *Adv. Funct. Mater.*, 2015, **25**, 427–436.

32 N. Matsuhisa, D. Inoue, P. Zalar, H. Jin, Y. Matsuba, A. Itoh, T. Yokota, D. Hashizume and T. Someya, *Nat. Mater.*, 2017, **16**, 834–840.

33 S. Wünscher, R. Abbel, J. Perelaer and U. S. Schubert, *J. Mater. Chem. C*, 2014, **2**, 10232–10261.

34 C. Jin, W. Liu, Y. Xu, Y. Huang, Y. Nie, X. Shi, G. Zhang, P. He, J. Zhang and H. Cao, *Nano Lett.*, 2022, **22**, 3372–3379.

35 M. Senel, M. Dervisevic and N. H. Voelcker, *Mater. Lett.*, 2019, **243**, 50–53.

36 K. Sim, Z. Rao, H.-J. Kim, A. Thukral, H. Shim and C. Yu, *Sci. Adv.*, 2019, **5**, eaav5749.

37 C. Jin, W. Liu, Y. Huang, Y. Xu, Y. Nie, G. Zhang, P. He, J. Sun and J. Yang, *Appl. Phys. Lett.*, 2022, **120**, 233701.

38 J. Krantz, M. Richter, S. Spallek, E. Spiecker and C. J. Brabec, *Adv. Funct. Mater.*, 2011, **21**, 4784–4787.

39 N. Matsuhisa, S. Niu, S. J. K. O'Neill, J. Kang, Y. Ochiai, T. Katsumata, H.-C. Wu, M. Ashizawa, G.-J. N. Wang, D. Zhong, X. Wang, X. Gong, R. Ning, H. Gong, I. You, Y. Zheng, Z. Zhang, J. B. H. Tok, X. Chen and Z. Bao, *Nature*, 2021, **600**, 246–252.

40 M. Hauder, J. Gstöttner, W. Hansch and D. Schmitt-Landsiedel, *Appl. Phys. Lett.*, 2001, **78**, 838–840.

41 M. Singh and S. Rana, *Mater. Today Commun.*, 2020, **24**, 101317.

42 D. R. Kumar, K. Woo and J. Moon, *Nanoscale*, 2015, **7**, 17195–17210.

43 K. Ankireddy, T. Druffel, S. Vunnam, G. Filipič, R. Dharmadasa and D. A. Amos, *J. Mater. Chem. C*, 2017, **5**, 11128–11137.

44 S. Zhao, F. Han, J. Li, X. Meng, W. Huang, D. Cao, G. Zhang, R. Sun and C. P. Wong, *Small*, 2018, **14**, 1800047.

45 W. Li, Q. Sun, L. Li, J. Jiu, X.-Y. Liu, M. Kanehara, T. Minari and K. Suganuma, *Appl. Mater. Today*, 2020, **18**, 100451.

46 D. Tomotoshi and H. Kawasaki, *Nanomaterials*, 2020, **10**, 1689.

47 K. Kondo, in *Copper Electrodeposition for Nanofabrication of Electronics Devices*, Springer, 2014, pp. 177–192.

48 J. Xue, J. Song, Y. Dong, L. Xu, J. Li and H. Zeng, *Sci. Bull.*, 2017, **62**, 143–156.

49 S. Ding and Y. Tian, *RSC Adv.*, 2019, **9**, 26961–26980.

50 X. Li, Y. Wang, C. Yin and Z. Yin, *J. Mater. Chem. C*, 2020, **8**, 849–872.

51 Y. Wang and Z. Yin, *Appl. Sci. Converg. Technol.*, 2019, **28**, 186–193.

52 W. Li, Y. Yang, B. Zhang, C. F. Li, J. Jiu and K. Suganuma, *Adv. Mater. Interfaces*, 2018, **5**, 1800798.

53 W. Li, L. Li, Y. Gao, D. Hu, C.-F. Li, H. Zhang, J. Jiu, S. Nagao and K. Suganuma, *J. Alloys Compd.*, 2018, **732**, 240–247.

54 J. Ryu, H.-S. Kim and H. T. Hahn, *J. Electron. Mater.*, 2011, **40**, 42–50.

55 K. Woo, D. Kim, J. S. Kim, S. Lim and J. Moon, *Langmuir*, 2009, **25**, 429–433.

56 B. K. Park, D. Kim, S. Jeong, J. Moon and J. S. Kim, *Thin Solid Films*, 2007, **515**, 7706–7711.

57 I. Kim, Y. Kim, K. Woo, E.-H. Ryu, K.-Y. Yon, G. Cao and J. Moon, *RSC Adv.*, 2013, **3**, 15169–15177.

58 P. E. Laibinis and G. M. Whitesides, *J. Am. Chem. Soc.*, 1992, **114**, 9022–9028.

59 M. P. Mihajlović and M. M. Antonijević, *Int. J. Electrochem. Sci.*, 2015, **10**, 1027–1053.

60 Z. Niu, F. Cui, Y. Yu, N. Becknell, Y. Sun, G. Khanarian, D. Kim, L. Dou, A. Dehestani and K. Schierle-Arndt, *J. Am. Chem. Soc.*, 2017, **139**, 7348–7354.

61 H. Zhang, Y. Tian, S. Wang, Y. Huang, J. Wen, C. Hang, Z. Zheng and C. Wang, *Chem. Eng. J.*, 2020, **399**, 125075.

62 Z. Zuo, F. He, F. Wang, L. Li and Y. Li, *Adv. Mater.*, 2020, **32**, 2004379.

63 S. Xiao, W. Dai, X. Liu, D. Pan, H. Zou, G. Li, G. Zhang, C. Su, D. Zhang and W. Chen, *Adv. Energy Mater.*, 2019, **9**, 1900775.

64 L. W. Yap, S. Gong, Y. Tang, Y. Zhu and W. Cheng, *Sci. Bull.*, 2016, **61**, 1624–1630.

65 T. öhlund, A. K. Schuppert, M. Hummelgard, J. Bäckström, H.-E. Nilsson and H. k. Olin, *ACS Appl. Mater. Interfaces*, 2015, **7**, 18273–18282.

66 S.-J. Oh, T. G. Kim, S.-Y. Kim, Y. Jo, S. S. Lee, K. Kim, B.-H. Ryu, J.-U. Park, Y. Choi and S. Jeong, *Chem. Mater.*, 2016, **28**, 4714–4723.

67 M. A. Cruz, S. Ye, M. J. Kim, C. Reyes, F. Yang, P. F. Flowers and B. J. Wiley, *Part. Part. Syst. Charact.*, 2018, **35**, 1700385.

68 Y. Fang, X. Zeng, Y. Chen, M. Ji, H. Zheng, W. Xu and D.-L. Peng, *Nanotechnology*, 2020, **31**, 355601.

69 B. F. Y. Rezaga and M. D. L. Balela, *Mater. Today: Proc.*, 2020, **22**, 241–247.

70 Y. Sui, C. A. Zorman and R. M. Sankaran, *Plasma Processes Polym.*, 2020, **17**, 2000009.

71 H. Abdolmaleki, P. Kidmose and S. Agarwala, *Adv. Mater.*, 2021, 2006792.

72 Y. Choi, K. d. Seong and Y. Piao, *Adv. Mater. Interfaces*, 2019, **6**, 1901002.

73 N. Raut and K. Al-Shamery, *J. Mater. Chem. C*, 2018, **6**, 1618–1641.

74 A. Oliva-Puigdomenech, J. De Roo, H. Van Avermaet, K. De Buysser and Z. Hens, *ACS Appl. Nano Mater.*, 2020, **3**, 3523–3531.

75 N. Hayati-Roodbari, A. Wheeldon, C. Hendler, A. Fian and R. Trattnig, *Nanotechnology*, 2021, **32**, 225205.

76 N. Sarwar, S. H. Choi, G. Dastgeer, U. B. Humayoun, M. Kumar, A. Nawaz, D. I. Jeong, S. F. A. Zaidi and D. H. Yoon, *Appl. Surf. Sci.*, 2021, **542**, 148609.

77 R. Deshmukh, M. Calvo, M. Schreck, E. Tervoort, A. S. Sologubenko and M. Niederberger, *ACS Appl. Mater. Interfaces*, 2018, **10**, 20748–20754.

78 M. B. Gawande, A. Goswami, F.-X. Felpin, T. Asefa, X. Huang, R. Silva, X. Zou, R. Zboril and R. S. Varma, *Chem. Rev.*, 2016, **116**, 3722–3811.

79 P. Karthik and S. P. Singh, *RSC Adv.*, 2015, **5**, 63985–64030.

80 A. Umer, S. Naveed, N. Ramzan and M. S. Rafique, *Nano*, 2012, **7**, 1230005.

81 D. Mott, J. Galkowski, L. Wang, J. Luo and C.-J. Zhong, *Langmuir*, 2007, **23**, 5740–5745.

82 X. Song, S. Sun, W. Zhang and Z. Yin, *J. Colloid Interface Sci.*, 2004, **273**, 463–469.

83 W. Songping and M. Shuyuan, *Mater. Lett.*, 2006, **60**, 2438–2442.

84 S. Saikova, S. Vorob'ev, R. Nikolaeva and Y. L. Mikhlin, *Russ. J. Gen. Chem.*, 2010, **80**, 1122–1127.

85 Y. Hokita, M. Kanzaki, T. Sugiyama, R. Arakawa and H. Kawasaki, *ACS Appl. Mater. Interfaces*, 2015, **7**, 19382–19389.

86 S. Jeong, H. C. Song, W. W. Lee, S. S. Lee, Y. Choi, W. Son, E. D. Kim, C. H. Paik, S. H. Oh and B.-H. Ryu, *Langmuir*, 2011, **27**, 3144–3149.

87 Y. Zhang, P. Zhu, G. Li, T. Zhao, X. Fu, R. Sun, F. Zhou and C.-p. Wong, *ACS Appl. Mater. Interfaces*, 2014, **6**, 560–567.

88 N. K. Roy, C. S. Foong and M. A. Cullinan, *Addit. Manuf.*, 2018, **21**, 17–29.

89 G. Allen, R. Bayles, W. Gile and W. Jesser, *Thin Solid Films*, 1986, **144**, 297–308.

90 S. Jeong, K. Woo, D. Kim, S. Lim, J. S. Kim, H. Shin, Y. Xia and J. Moon, *Adv. Funct. Mater.*, 2008, **18**, 679–686.

91 S. Yokoyama, J. Nozaki, K. Motomiya, N. Tsukahara and H. Takahashi, *Colloids Surf., A*, 2020, **591**, 124567.

92 Y. Li, X. Tang, Y. Zhang, J. Li, C. Lv, X. Meng, Y. Huang, C. Hang and C. Wang, *Colloid Polym. Sci.*, 2014, **292**, 715–722.

93 S.-J. Oh, Y. Jo, E. J. Lee, S. S. Lee, Y. H. Kang, H.-J. Jeon, S. Y. Cho, J.-S. Park, Y.-H. Seo and B.-H. Ryu, *Nanoscale*, 2015, **7**, 3997–4004.

94 Y. Son, D. Shin, M. Kang and C. S. Lee, *Electron. Mater.*, 2020, **1**, 28–39.

95 Y.-H. Son, J.-Y. Jang, M. K. Kang, S. Ahn and C. S. Lee, *Thin Solid Films*, 2018, **656**, 61–67.

96 T. G. Kim, H. J. Park, K. Woo, S. Jeong, Y. Choi and S. Y. Lee, *ACS Appl. Mater. Interfaces*, 2018, **10**, 1059–1066.

97 A. Sheng, S. Khuje, J. Yu, T. Parker, J.-Y. Tsai, L. An, Y. Huang, Z. Li, C.-G. Zhuang and L. Kester, *ACS Appl. Nano Mater.*, 2022, **5**, 4028–4037.

98 H.-J. Huang, M.-B. Zhou and X.-P. Zhang, *ACS Appl. Electron. Mater.*, 2021, **3**, 4640–4648.

99 D. Deng, Y. Jin, Y. Cheng, T. Qi and F. Xiao, *ACS Appl. Mater. Interfaces*, 2013, **5**, 3839–3846.

100 W. Li, M. Chen, J. Wei, W. Li and C. You, *J. Nanopart. Res.*, 2013, **15**, 1–10.

101 G. D. M. R. Dabera, M. Walker, A. M. Sanchez, H. J. Pereira, R. Beanland and R. A. Hatton, *Nat. Commun.*, 2017, **8**, 1–10.

102 S. Wu, *Mater. Lett.*, 2007, **61**, 1125–1129.

103 J. Moghimi-Rad, F. Zabihi, I. Hadi, S. Ebrahimi, T. D. Isfahani and J. Sabbaghzadeh, *J. Mater. Sci.*, 2010, **45**, 3804–3811.

104 S. Shiomi, M. Kawamori, S. Yagi and E. Matsubara, *J. Colloid Interface Sci.*, 2015, **460**, 47–54.

105 C. Wang, H. Cheng, Y. Huang, Z. Xu, H. Lin and C. Zhang, *Analyst*, 2015, **140**, 5634–5639.

106 C. Schmädicke, M. Poetschke, L. Renner, L. Baraban, M. Bobeth and G. Cuniberti, *RSC Adv.*, 2014, **4**, 46363–46368.

107 H. Qiu, S. Xu, P. Chen, S. Gao, Z. Li, C. Zhang, S. Jiang, M. Liu, H. Li and D. Feng, *Appl. Surf. Sci.*, 2015, **332**, 614–619.

108 M. Nasrollahzadeh, S. M. Sajadi and M. Khalaj, *RSC Adv.*, 2014, **4**, 47313–47318.

109 G. G. Jang, C. B. Jacobs, R. G. Gresback, I. N. Ivanov, H. M. Meyer III, M. Kidder, P. C. Joshi, G. E. Jellison, T. J. Phelps and D. E. Graham, *J. Mater. Chem. C*, 2015, **3**, 644–650.

110 H.-J. Yang, S.-Y. He, H.-L. Chen and H.-Y. Tuan, *Chem. Mater.*, 2014, **26**, 1785–1793.

111 H.-J. Huang, M.-B. Zhou, C. Yin, Q.-W. Chen and X.-P. Zhang, 2018 19th International Conference on Electronic Packaging Technology (ICEPT), 2018, pp. 491–495.

112 S. Hong, C. Liu, S. Hao, W. Fu, J. Peng, B. Wu and N. Zheng, *npj Flexible Electron.*, 2022, **6**, 1–9.

113 C.-H. Lu, C.-M. Leu and N.-C. Yeh, *ACS Appl. Mater. Interfaces*, 2021, **13**, 6951–6959.

114 J. W. Lee, J. H. Kwak, J. Kim, S. Jeong, J. H. Park, S. Y. Jeong, S. H. Seo, J. T. Han, G. W. Lee and K. J. Baeg, *Adv. Mater. Interfaces*, 2021, **8**, 2100769.

115 A. Luce, G. Strack, O. Ranasingha, E. Kingsely, C. Armiento and A. Akyurtlu, *MRS Adv.*, 2020, **5**, 2191–2199.

116 H. Y. Jun, E. J. Lee and S. O. Ryu, *Curr. Appl. Phys.*, 2020, **20**, 853–861.

117 T. T. T. Can, T. C. Nguyen and W.-S. Choi, *Adv. Eng. Mater.*, 2020, **22**, 1901384.

118 B. H. Teo, A. Khanna, V. Shanmugam, M. L. O. Aguilar, M. E. D. Santos, D. J. W. Chua, W.-C. Chang and T. Mueller, *Sol. Energy*, 2019, **189**, 179–185.

119 C. Lee, N. R. Kim, J. Koo, Y. J. Lee and H. M. Lee, *Nanotechnology*, 2015, **26**, 455601.

120 G. Kawamura, S. Alvarez, I. E. Stewart, M. Catenacci, Z. Chen and Y.-C. Ha, *Sci. Rep.*, 2015, **5**, 1–8.

121 A. Zareei, S. Gopalakrishnan, Z. Mutlu, Z. He, S. Peana, H. Wang and R. Rahimi, *ACS Appl. Electron. Mater.*, 2021, **3**, 3352–3364.

122 S. Yokoyama, J. Nozaki, Y. Umemoto, K. Motomiya, T. Itoh and H. Takahashi, *Colloids Surf., A*, 2021, **652**, 126907.

123 D. Tomotoshi, R. Oogami and H. Kawasaki, *ACS Appl. Mater. Interfaces*, 2021, **13**, 20906–20915.

124 Y.-R. Jang, R. Jeong, H.-S. Kim and S. S. Park, *Sci. Rep.*, 2021, **11**, 1–15.

125 B. Zhang, C. Chen, W. Li, J. Yeom and K. Suganuma, *Adv. Mater. Interfaces*, 2020, **7**, 1901550.

126 C.-H. Ryu, H.-J. Um and H.-S. Kim, *Thin Solid Films*, 2020, **701**, 137951.

127 W. Li, L. Li, F. Li, K. Kawakami, Q. Sun, T. Nakayama, X. Liu, M. Kanehara, J. Zhang and T. Minari, *ACS Appl. Mater. Interfaces*, 2022, **14**, 8146–8156.

128 C.-H. Ryu, S.-J. Joo and H.-S. Kim, *Thin Solid Films*, 2019, **675**, 23–33.

129 J.-H. Chu, S.-J. Joo and H.-S. Kim, *Thin Solid Films*, 2019, **680**, 1–11.

130 K. d. Seong, J. M. Kim, J. Kang, M. Hwang, C. Lee and Y. Piao, *Adv. Mater. Interfaces*, 2018, **5**, 1800502.

131 X. Chen, X. Wu, S. Shao, J. Zhuang, L. Xie, S. Nie, W. Su, Z. Chen and Z. Cui, *Sci. Rep.*, 2017, **7**, 13239.

132 W. Li, S. Cong, J. Jiu, S. Nagao and K. Suganuma, *J. Mater. Chem. C*, 2016, **4**, 8802–8809.

133 W.-H. Chung, Y.-T. Hwang, S.-H. Lee and H.-S. Kim, *Nanotechnology*, 2016, **27**, 205704.

134 X. Dai, W. Xu, T. Zhang, H. Shi and T. Wang, *Chem. Eng. J.*, 2019, **364**, 310–319.

135 W. Yang, C. Wang and V. Arrighi, *J. Mater. Sci.: Mater. Electron.*, 2019, **30**, 11607–11618.

136 K. Woo, Y. Kim, B. Lee, J. Kim and J. Moon, *ACS Appl. Mater. Interfaces*, 2011, **3**, 2377–2382.

137 D. Deng, Y. Cheng, Y. Jin, T. Qi and F. Xiao, *J. Mater. Chem.*, 2012, **22**, 23989–23995.

138 M. J. Schadt, W. Cheung, J. Luo and C.-J. Zhong, *Chem. Mater.*, 2006, **18**, 5147–5149.

139 H.-X. Zhang, U. Siegert, R. Liu and W.-B. Cai, *Nanoscale Res. Lett.*, 2009, **4**, 705–708.

140 S. Casalini, C. A. Bortolotti, F. Leonardi and F. Biscarini, *Chem. Soc. Rev.*, 2017, **46**, 40–71.

141 P. Kanninen, C. Johans, J. Merta and K. Kontturi, *J. Colloid Interface Sci.*, 2008, **318**, 88–95.

142 Z. Li, S. Chang, S. Khuje and S. Ren, *ACS Nano*, 2021, **15**, 6211–6232.

143 A. R. Rathmell and B. J. Wiley, *Adv. Mater.*, 2011, **23**, 4798–4803.

144 S. Ye, I. E. Stewart, Z. Chen, B. Li, A. R. Rathmell and B. J. Wiley, *Acc. Chem. Res.*, 2016, **49**, 442–451.

145 S. Bhanushali, P. Ghosh, A. Ganesh and W. Cheng, *Small*, 2015, **11**, 1232–1252.

146 V. B. Nam and D. Lee, *Nanomaterials*, 2016, **6**, 47.

147 H.-G. Im, S.-H. Jung, J. Jin, D. Lee, J. Lee, D. Lee, J.-Y. Lee, I.-D. Kim and B.-S. Bae, *ACS Nano*, 2014, **8**, 10973–10979.

148 C. Sachse, N. Weiß, N. Gaponik, L. Müller-Meskamp, A. Eychmüller and K. Leo, *Adv. Energy Mater.*, 2014, **4**, 1300737.

149 T.-H. Duong and H.-C. Kim, *Ind. Eng. Chem. Res.*, 2018, **57**, 3076–3082.

150 Z. Li, S. Khuje, A. Chivate, Y. Huang, Y. Hu, L. An, Z. Shao, J. Wang, S. Chang and S. Ren, *ACS Appl. Electron. Mater.*, 2020, **2**, 1867–1873.

151 J. Kim, I. Hwang, M. Kim, H. Jung, H. Bae and Y. Lee, *ACS Appl. Mater. Interfaces*, 2022, **14**, 5807–5814.

152 A. R. Rathmell, S. M. Bergin, Y. L. Hua, Z. Y. Li and B. J. Wiley, *Adv. Mater.*, 2010, **22**, 3558–3563.

153 J. W. Borchert, I. E. Stewart, S. Ye, A. R. Rathmell, B. J. Wiley and K. I. Winey, *Nanoscale*, 2015, **7**, 14496–14504.

154 F. Meng and S. Jin, *Nano Lett.*, 2012, **12**, 234–239.

155 S. Yu, Z. Liu, L. Zhao and B. Gong, *Opt. Mater.*, 2021, **119**, 111301.

156 Y. Shi, H. Li, L. Chen and X. Huang, *Sci. Technol. Adv. Mater.*, 2005, **6**, 761–765.

157 Y. Wang, P. Liu, B. Zeng, L. Liu and J. Yang, *Nanoscale Res. Lett.*, 2018, **13**, 1–10.

158 N.-H. Tran, D.-A. Nguyen, T.-H. Duong and H.-C. Kim, *Thin Solid Films*, 2019, **685**, 26–33.

159 J. L. Cuya Huaman, I. Urushizaki and B. Jeyadevan, *J. Nanomater.*, 2018, **2018**, 1698357.

160 Z. Zhong, K. Woo, I. Kim, H. Hwang, S. Kwon, Y.-M. Choi, Y. Lee, T.-M. Lee, K. Kim and J. Moon, *Nanoscale*, 2016, **8**, 8995–9003.

161 S.-S. Chee, H. Kim, M. Son and M.-H. Ham, *Electron. Mater. Lett.*, 2020, **16**, 404–410.

162 T. I. Kim, I.-J. Park and S.-Y. Choi, *Nano Lett.*, 2020, **20**, 3740–3746.

163 Y. Won, A. Kim, W. Yang, S. Jeong and J. Moon, *NPG Asia Mater.*, 2014, **6**, e132–e132.

164 M. Bobinger, J. Mock, P. La Torraca, M. Becherer, P. Lugli and L. Larcher, *Adv. Mater. Interfaces*, 2017, **4**, 1700568.

165 M. Bobinger, P. La Torraca, J. Mock, M. Becherer, L. Cattani, D. Angeli, L. Larcher and P. Lugli, *IEEE Trans. Nanotechnol.*, 2018, **17**, 940–947.

166 J. Mock, M. Bobinger, C. Bogner, P. Lugli and M. Becherer, *Nanomaterials*, 2018, **8**, 767.

167 A. S. Hashimi, R. T. Ginting, S. X. Chin, K. S. Lau, M. A. N. M. Nohan, S. Zakaria, C. C. Yap and C. H. Chia, *Curr. Appl. Phys.*, 2020, **20**, 205–211.

168 S. Polat Genlik, D. Tigan, Y. Kocak, K. E. Ercan, M. O. Cicek, S. Tunca, S. Koylan, S. Coskun, E. Ozensoy and H. E. Unalan, *ACS Appl. Mater. Interfaces*, 2020, **12**, 45136–45144.

169 N.-H. Tran, H.-M. Hoang, T.-H. Duong and H.-C. Kim, *Appl. Surf. Sci.*, 2020, **520**, 146216.

170 J. Wang, Z. Zhang, S. Wang, R. Zhang, Y. Guo, G. Cheng, Y. Gu, K. Liu and K. Chen, *Nano Energy*, 2020, **71**, 104638.

171 H. Yang, H.-C. Kwon, S. Ma, K. Kim, S.-C. Yun, G. Jang, J. Park, H. Lee, S. Goh and J. Moon, *ACS Appl. Mater. Interfaces*, 2020, **12**, 13824–13835.

172 Y. Dong, Z. Lin, X. Li, Q. Zhu, J.-G. Li and X. Sun, *J. Mater. Chem. C*, 2018, **6**, 6406–6415.

173 Y. S. Rosen, A. Yakushenko, A. Offenhäusser and S. Magdassi, *ACS Omega*, 2017, **2**, 573–581.

174 J. Montes, J. Rodriguez and E. Herrera, *Powder Metall.*, 2003, **46**, 251–256.

175 A. Yabuki, S. Kawahara, S. Kang and I. W. Fathona, *Mater. Sci. Eng., B*, 2020, **262**, 114743.

176 Y. Rosen, R. Marrach, V. Gutkin and S. Magdassi, *Adv. Mater. Technol.*, 2019, **4**, 1800426.

177 Y. Farraj, M. Grouchko and S. Magdassi, *Chem. Commun.*, 2015, **51**, 1587–1590.

178 S. J. Kim, J. Lee, Y.-H. Choi, D.-H. Yeon and Y. Byun, *Thin Solid Films*, 2012, **520**, 2731–2734.

179 Y.-H. Choi and S.-H. Hong, *Langmuir*, 2015, **31**, 8101–8110.

180 C. Paquet, T. Lacelle, X. Liu, B. Deore, A. J. Kell, S. Lafrenière and P. R. Malenfant, *Nanoscale*, 2018, **10**, 6911–6921.

181 H. Shin, X. Liu, T. Lacelle, R. J. MacDonell, M. S. Schuurman, P. R. L. Malenfant and C. Paquet, *ACS Appl. Mater. Interfaces*, 2020, **12**, 33039–33049.

182 M. S. Rager, T. Aytug, G. M. Veith and P. Joshi, *ACS Appl. Mater. Interfaces*, 2016, **8**, 2441–2448.

183 S. Oldenhof, M. Lutz, B. de Bruin, J. I. van der Vlugt and J. N. Reek, *Chem. Sci.*, 2015, **6**, 1027–1034.

184 A. Nova, D. J. Taylor, A. J. Blacker, S. B. Duckett, R. N. Perutz and O. Eisenstein, *Organometallics*, 2014, **33**, 3433–3442.

185 Y. Huang, X. Xie, M. Li, M. Xu and J. Long, *Opt. Express*, 2021, **29**, 4453–4463.

186 C. Paquet, R. James, A. J. Kell, O. Mozenson, J. Ferrigno, S. Lafrenière and P. R. Malenfant, *Org. Electron.*, 2014, **15**, 1836–1842.

187 M. K. Rahman, Z. Lu and K.-S. Kwon, *AIP Adv.*, 2018, **8**, 095008.

188 S. Kang, K. Tasaka, J. H. Lee and A. Yabuki, *Chem. Phys. Lett.*, 2021, **763**, 138248.

189 J.-J. Chen, G.-Q. Lin, Y. Wang, E. Sowade, R. R. Baumann and Z.-S. Feng, *Appl. Surf. Sci.*, 2017, **396**, 202–207.

190 S. Bai, S. Zhang, W. Zhou, D. Ma, Y. Ma, P. Joshi and A. Hu, *Nano-Micro Lett.*, 2017, **9**, 42.

191 Y.-T. Kwon, Y.-S. Kim, Y. Lee, S. Kwon, M. Lim, Y. Song, Y.-H. Choa and W.-H. Yeo, *ACS Appl. Mater. Interfaces*, 2018, **10**, 44071–44079.

192 Y. Guo, H. Cai, Z. Wang, X. Wang, P. Cao, P. Chen and Y. Wang, *Mater. Lett.*, 2021, **286**, 129234.

193 Y. Li, T. Qi, M. Chen and F. Xiao, *J. Mater. Sci.: Mater. Electron.*, 2016, **27**, 11432–11438.

194 Y. H. Jo, I. Jung, C. S. Choi, I. Kim and H. M. Lee, *Nanotechnology*, 2011, **22**, 225701.

195 Z. Shi, J. Sheng, Z. Yang, Z. Liu, S. Chen, M. Wang, L. Wang and W. Fei, *Carbon*, 2020, **165**, 349–357.

196 H. B. Lee, C. W. Bae, L. T. Duy, I. Y. Sohn, D. I. Kim, Y. J. Song, Y. J. Kim and N. E. Lee, *Adv. Mater.*, 2016, **28**, 3069–3077.

197 J. Joo, B. Y. Chow and J. M. Jacobson, *Nano Lett.*, 2006, **6**, 2021–2025.

198 C. W. Chen, H. W. Kang, S. Y. Hsiao, P. F. Yang, K. M. Chiang and H. W. Lin, *Adv. Mater.*, 2014, **26**, 6647–6652.

199 D. Zhuang and J. Edgar, *Mater. Sci. Eng., R*, 2005, **48**, 1–46.

200 A. Z. Qamar and M. H. Shamsi, *Micromachines*, 2020, **11**, 126.

201 M. Pudas, N. Halonen, P. Granat and J. Vähäkangas, *Prog. Org. Coat.*, 2005, **54**, 310–316.

202 D. Kim, S. Jeong, J. Moon and K. Kang, *Mol. Cryst. Liq. Cryst.*, 2006, **459**, 45/[325]–355/[335].

203 S. Merilampi, T. Laine-Ma and P. Ruuskanen, *Microelectron. Reliab.*, 2009, **49**, 782–790.

204 G. Mattana, A. Loi, M. Woytasik, M. Barbaro, V. Noël and B. Piro, *Adv. Mater. Technol.*, 2017, **2**, 1700063.

205 P. He and B. Derby, *2D Mater.*, 2017, **4**, 021021.

206 K. Kim, S. I. Ahn and K. C. Choi, *Curr. Appl. Phys.*, 2013, **13**, 1870–1873.

207 B. Bao, J. Jiang, F. Li, P. Zhang, S. Chen, Q. Yang, S. Wang, B. Su, L. Jiang and Y. Song, *Adv. Funct. Mater.*, 2015, **25**, 3286–3294.

208 J. Sun, B. Bao, M. He, H. Zhou and Y. Song, *ACS Appl. Mater. Interfaces*, 2015, **7**, 28086–28099.

209 Y. Sui, Y. Dai, C. C. Liu, R. M. Sankaran and C. A. Zorman, *Adv. Mater. Technol.*, 2019, **4**, 1900119.

210 B. Derby, *Annu. Rev. Mater. Res.*, 2010, **40**, 395–414.

211 L. Siebert, N. Wolff, N. Ababii, M.-I. Terasa, O. Lupan, A. Vahl, V. Duppel, H. Qiu, M. Tienken and M. Mirabelli, *Nano Energy*, 2020, **70**, 104420.

212 Z. Zhong, H. Lee, D. Kang, S. Kwon, Y.-M. Choi, I. Kim, K.-Y. Kim, Y. Lee, K. Woo and J. Moon, *ACS Nano*, 2016, **10**, 7847–7854.

213 X. Xu, G. Han, H. Yu, X. Jin, J. Yang, J. Lin and C. Ma, *J. Phys. D: Appl. Phys.*, 2019, **53**, 05LT02.

214 D. J. Finn, M. Lotya and J. N. Coleman, *ACS Appl. Mater. Interfaces*, 2015, **7**, 9254–9261.

215 Q. Huang, K. N. Al-Milaji and H. Zhao, *ACS Appl. Nano Mater.*, 2018, **1**, 4528–4536.

216 S. Liu, Y. Li, S. Xing, L. Liu, G. Zou and P. Zhang, *Materials*, 2019, **12**, 1559.

217 S. Khuje, A. Sheng, J. Yu and S. Ren, *ACS Appl. Electron. Mater.*, 2021, **3**, 5468–5474.

218 H. Yuk and X. Zhao, *Adv. Mater.*, 2018, **30**, 1704028.

219 M. Zhu, Y. Duan, N. Liu, H. Li, J. Li, P. Du, Z. Tan, G. Niu, L. Gao and Y. Huang, *Adv. Funct. Mater.*, 2019, **29**, 1903294.

220 J.-U. Park, M. Hardy, S. J. Kang, K. Barton, K. Adair, C. Y. Lee, M. S. Strano, A. G. Alleyne, J. G. Georgiadis and P. M. Ferreira, *Nat. Mater.*, 2007, **6**, 782–789.

221 K. Kim, G. Kim, B. R. Lee, S. Ji, S.-Y. Kim, B. W. An, M. H. Song and J.-U. Park, *Nanoscale*, 2015, **7**, 13410–13415.

222 S.-Y. Kim, K. Kim, Y. Hwang, J. Park, J. Jang, Y. Nam, Y. Kang, M. Kim, H. Park and Z. Lee, *Nanoscale*, 2016, **8**, 17113–17121.

223 D. Ye, Y. Ding, Y. Duan, J. Su, Z. Yin and Y. A. Huang, *Small*, 2018, **14**, 1703521.

224 R. Durairaj, S. Ramesh, S. Mallik, A. Seman and N. Ekere, *Mater. Des.*, 2009, **30**, 3812–3818.

225 K.-i. Nomura, H. Ushijima, R. Mitsui, S. Takahashi and S.-i. Nakajima, *Microelectron. Eng.*, 2014, **123**, 58–61.

226 X. Xu, Z. Liu, P. He and J. Yang, *J. Phys. D: Appl. Phys.*, 2019, **52**, 455401.

227 X. Xu, M. Luo, P. He and J. Yang, *J. Phys. D: Appl. Phys.*, 2020, **53**, 125402.

228 K.-i. Nomura, Y. Kusaka, H. Ushijima, K. Nagase, H. Ikedo, R. Mitsui, S. Takahashi, S.-i. Nakajima and S. Iwata, *J. Micromech. Microeng.*, 2014, **24**, 095021.

229 O. P. Falade, S. F. Jilani, A. Y. Ahmed, T. Wildsmith, P. Reip, K. Z. Rajab and A. Alomainy, *Flexible Printed Electron.*, 2018, **3**, 045005.

230 I. Kim, S.-W. Kwak, K.-S. Kim, T.-M. Lee, J. Jo, J.-H. Kim and H.-J. Lee, *Microelectron. Eng.*, 2012, **98**, 587–589.

231 J. Johnson, *Aspects of flexographic print quality and relationship to some printing parameters*, Karlstad University, 2008.

232 J. D. Park, S. Lim and H. Kim, *Thin Solid Films*, 2015, **586**, 70–75.

233 X. M. Zhang, X.-L. Yang and B. Wang, *J. Mater. Sci.: Mater. Electron.*, 2022, **33**, 8096–8103.

234 M. Yuan, J. Xu, Q. Chen, D. Li and D. Yang, *J. Mater. Sci.: Mater. Electron.*, 2018, **29**, 14989–14994.

235 D. Li, W. Y. Lai, Y. Z. Zhang and W. Huang, *Adv. Mater.*, 2018, **30**, 1704738.

236 H.-J. Hwang, K.-H. Oh and H.-S. Kim, *Sci. Rep.*, 2016, **6**(1), 1–10.

237 G.-H. Oh, H.-J. Hwang and H.-S. Kim, *RSC Adv.*, 2017, **7**, 17724–17731.

238 Y. Gao, H. Zhang, J. Jiu, S. Nagao, T. Sugahara and K. Suganuma, *RSC Adv.*, 2015, **5**, 90202–90208.

239 Y. Jo, H. J. Park, Y. B. Kim, S. S. Lee, S. Y. Lee, S. K. Kim, Y. Choi and S. Jeong, *Adv. Funct. Mater.*, 2020, **30**, 2004659.

240 Y. Son, J. Yeo, H. Moon, T. W. Lim, S. Hong, K. H. Nam, S. Yoo, C. P. Grigoropoulos, D. Y. Yang and S. H. Ko, *Adv. Mater.*, 2011, **23**, 3176–3181.

241 H.-S. Kim, S. R. Dhage, D.-E. Shim and H. T. Hahn, *Appl. Phys. A*, 2009, **97**, 791–798.

242 B. Kang, S. Hong, C. Yoo, D. You, Y.-W. Ma, S. M. Lee, M.-W. Kim, M. H. Kim and B. S. Shin, *Appl. Phys. A*, 2018, **124**, 1–5.

243 D. Tobjörk, H. Aarnio, P. Pulkkinen, R. Bollström, A. Määttänen, P. Ihalainen, T. Mäkelä, J. Peltonen, M. Toivakka and H. Tenhu, *Thin Solid Films*, 2012, **520**, 2949–2955.

244 E.-B. Jeon, S.-J. Joo, H. Ahn and H.-S. Kim, *Thin Solid Films*, 2016, **603**, 382–390.

245 J. Niittynen, E. Sowade, H. Kang, R. R. Baumann and M. Mäntysalo, *Sci. Rep.*, 2015, **5**, 1–10.

246 K. Mallikarjuna, H.-J. Hwang, W.-H. Chung and H.-S. Kim, *RSC Adv.*, 2016, **6**, 4770–4779.

247 M. A. Rafea and N. Roushdy, *J. Phys. D: Appl. Phys.*, 2008, **42**, 015413.

248 B. Kang, S. Han, J. Kim, S. Ko and M. Yang, *J. Phys. Chem. C*, 2011, **115**, 23664–23670.

249 S. Han, S. Hong, J. Yeo, D. Kim, B. Kang, M. Y. Yang and S. H. Ko, *Adv. Mater.*, 2015, **27**, 6397–6403.

250 Y.-J. Kim, C.-H. Ryu, S.-H. Park and H.-S. Kim, *Thin Solid Films*, 2014, **570**, 114–122.

251 M. Zenou, O. Ermak, A. Saar and Z. Kotler, *J. Phys. D: Appl. Phys.*, 2013, **47**, 025501.

252 S. Han, S. Hong, J. Ham, J. Yeo, J. Lee, B. Kang, P. Lee, J. Kwon, S. S. Lee and M. Y. Yang, *Adv. Mater.*, 2014, **26**, 5808–5814.

253 C.-W. Cheng and J. Chen, *Appl. Phys. A*, 2016, **122**, 1–8.

254 J. H. Park, S. Jeong, E. J. Lee, S. S. Lee, J. Y. Seok, M. Yang, Y. Choi and B. Kang, *Chem. Mater.*, 2016, **28**, 4151–4159.

255 S. Hong, H. Lee, J. Yeo and S. H. Ko, *Nano Today*, 2016, **11**, 547–564.

256 Z. Wang, W. Guo, L. Li, B. Luk'yanchuk, A. Khan, Z. Liu, Z. Chen and M. Hong, *Nat. Commun.*, 2011, **2**, 218.

257 A. Darafsheh, N. I. Limberopoulos, J. S. Derov, D. E. Walker and V. N. Astratov, *Appl. Phys. Lett.*, 2014, **104**, 061117.

258 X. Hao, C. Kuang, X. Liu, H. Zhang and Y. Li, *Appl. Phys. Lett.*, 2011, **99**, 203102.

259 M. Abedi, A. Asadi, S. Vorotilo and A. S. Mukasyan, *J. Mater. Sci.*, 2021, **56**, 19739–19766.

260 Y.-T. Kwon, Y.-I. Lee, S. Kim, K.-J. Lee and Y.-H. Choa, *Appl. Surf. Sci.*, 2017, **396**, 1239–1244.

261 C. E. Knapp, E. A. Metcalf, S. Mrig, C. Sanchez-Perez, S. P. Douglas, P. Choquet and N. D. Boscher, *ChemistryOpen*, 2018, **7**, 850–857.

262 K.-S. Kim, J.-O. Bang, Y.-H. Choa and S.-B. Jung, *Microelectron. Eng.*, 2013, **107**, 121–124.

263 Y. Farraj, A. Smooha, A. Kamyshny and S. Magdassi, *ACS Appl. Mater. Interfaces*, 2017, **9**, 8766–8773.

264 E. Redondo and M. Pumera, *Appl. Mater. Today*, 2021, **25**, 101253.

265 F. Hermerschmidt, D. Burmeister, G. Ligorio, S. M. Pozov, R. Ward, S. A. Choulis and E. J. List-Kratochvil, *Adv. Mater. Technol.*, 2018, **3**, 1800146.

266 S. Zhang, C. Wang, L. Ding, L. Zhang, J. Chen, H. Huang, D. Jiang, Z. Chen and G. Pan, *J. Mater. Chem. C*, 2020, **8**, 4081–4092.

267 Z. Chen, S. Ye, I. E. Stewart and B. J. Wiley, *ACS Nano*, 2014, **8**, 9673–9679.

268 N. K. Allam, A. A. Nazeer and E. A. Ashour, *J. Appl. Electrochem.*, 2009, **39**, 961–969.

269 C. Cui, A. T. O. Lim and J. Huang, *Nat. Nanotechnol.*, 2017, **12**, 834–835.

270 A. Fateh, M. Aliofkhazraei and A. Rezvanian, *Arabian J. Chem.*, 2020, **13**, 481–544.

271 V. Brusic, M. Frisch, B. Eldridge, F. Novak, F. Kaufman, B. Rush and G. Frankel, *J. Electrochem. Soc.*, 1991, **138**, 2253.

272 J. Zhou, X. Niu, Y. Cui, Z. Wang, J. Wang and R. Wang, *Appl. Surf. Sci.*, 2020, **505**, 144507.

273 J. Peng, B. Chen, Z. Wang, J. Guo, B. Wu, S. Hao, Q. Zhang, L. Gu, Q. Zhou, Z. Liu, S. Hong, S. You, A. Fu, Z. Shi, H. Xie, D. Cao, C.-J. Lin, G. Fu, L.-S. Zheng, Y. Jiang and N. Zheng, *Nature*, 2020, **586**, 390–394.

274 J. Peng, B. Chen, Z. Wang, J. Guo, B. Wu, S. Hao, Q. Zhang, L. Gu, Q. Zhou and Z. Liu, *Nature*, 2020, **586**, 390–394.

275 L. Zhao, S. Yu, X. Li, M. Wu and L. Li, *Sol. Energy Mater. Sol. Cells*, 2019, **201**, 110067.

276 D. Tigan, S. P. Genlik, B. Imer and H. E. Unalan, *Nanotechnology*, 2019, **30**, 325202.

277 D. S. Jung, H. Y. Koo, S. E. Wang, S. B. Park and Y. C. Kang, *Acta Mater.*, 2021, **206**, 116569.

278 I. E. Stewart, S. Ye, Z. Chen, P. F. Flowers and B. J. Wiley, *Chem. Mater.*, 2015, **27**, 7788–7794.

279 I. Hong, Y. Roh, J. S. Koh, S. Na, T. Kim, E. Lee, H. An, J. Kwon, J. Yeo and S. Hong, *Adv. Mater. Technol.*, 2019, **4**, 1800422.

280 Y. Ma, B. Fan, H. Liu, G. Fan, H. Hao and B. Yang, *Appl. Surf. Sci.*, 2020, **514**, 146086.

281 H. Zhang, S. Wang, C. Hang and Y. Tian, *Weld. World*, 2021, **65**, 1021–1030.

282 D. Kim, L. Zhu, D.-J. Jeong, K. Chun, Y.-Y. Bang, S.-R. Kim, J.-H. Kim and S.-K. Oh, *Carbon*, 2013, **63**, 530–536.

283 J. Kwon, H. Cho, H. Eom, H. Lee, Y. D. Suh, H. Moon, J. Shin, S. Hong and S. H. Ko, *ACS Appl. Mater. Interfaces*, 2016, **8**, 11575–11582.

284 W. Zhang, Z. Yin, A. Chun, J. Yoo, Y. S. Kim and Y. Piao, *ACS Appl. Mater. Interfaces*, 2016, **8**, 1733–1741.

285 X. Li, H.-j. Kwon, X. Qi, H. K. Choi, S. Lim, T.-W. Kim and S. H. Kim, *J. Ind. Eng. Chem.*, 2020, **85**, 269–275.

286 E. Georgiou, S. A. Choulis, F. Hermerschmidt, S. M. Pozov, I. Burgués-Ceballos, C. Christodoulou, G. Schider, S. Kreissl, R. Ward and E. J. List-Kratochvil, *Sol. RRL*, 2018, **2**, 1700192.

287 S. M. Pozov, G. Schider, S. Voigt, F. Ebert, K. Popovic, F. Hermerschmidt, E. Georgiou, I. Burgués-Ceballos, L. Kinner and D. Nees, *Flexible Printed Electron.*, 2019, **4**, 025004.

288 T. Kamijo, S. de Winter, P. Panditha and E. Meulenkamp, *ACS Appl. Electron. Mater.*, 2022, **4**, 698–706.

289 R. A. Street, *Adv. Mater.*, 2009, **21**, 2007–2022.

290 P. Xie, T. Liu, J. Sun, J. Jiang, Y. Yuan, Y. Gao, J. Zhou and J. Yang, *Sci. Bull.*, 2020, **65**, 791–795.

291 W. Liu, J. Sun, W. Qiu, Y. Chen, Y. Huang, J. Wang and J. Yang, *Nanoscale*, 2019, **11**, 21740–21747.

292 W. Qiu, J. Sun, W. Liu, Y. Huang, Y. Chen, J. Yang and Y. Gao, *Org. Electron.*, 2020, **84**, 105810.

293 S. P. Sreenilayam, I. U. Ahad, V. Nicolosi, V. A. Garzon and D. Brabazon, *Mater. Today*, 2020, **32**, 147–177.

294 M. Su and Y. Song, *Chem. Rev.*, 2021, **122**, 5144–5164.

295 **https://www.idtechex.com/en/research/webinars**.